Scintillation/dynamics of the signal

Document Version:
Publisher's PDF, also known as Version of Record (includes final page, issue and volume numbers)

Please check the document version of this publication:

• A submitted manuscript is the version of the article upon submission and before peer-review. There can be important differences between the submitted version and the official published version of record. People interested in the research are advised to contact the author for the final version of the publication, or visit the DOI to the publisher's website.
• The final author version and the galley proof are versions of the publication after peer review.
• The final published version features the final layout of the paper including the volume, issue and page numbers.

[Link to publication](#)

CHAPTER 2.3
Scintillation/Dynamics of the signal

Editor: Danielle Vanhoenacker[1]

Authors: Marie Edith Gimonet[2], Max M.J.L. van de Kamp[3], Frank S. Marzano[4], Carlo Riva[5], Errki Salonen[6]

[1] Universite Catholique de Louvain, Place du Levant 3, B-1348 Louvain-la-Neuve, Belgium
        Tel: +32-10-47-2304, Fax: +32-10-47-8705, e-mail: hoenacke@emic.ucl.ac.be

[2] ONERA-CERT DEMR, 2 Avenue Edouard Belin, BP4025, F-31055 Toulouse , CEDEX 4 France
        Tel: +33-562-25-2720 Fax: +33-562-25-2577 e-mail: Marie-Edith.Gimonet@onecert.fr

[3] Eindhoven University of Technology, P.O. Box 513, 5600 MB Eindhoven, The Netherlands
        Tel.: +31 40 247 2326, Fax.: +31 40 245 5197, e-mail: m.m.j.l.v.d.kamp@ele.tue.nl

[4] Dip. di Ingegneria Elettrica, Universita' dell'Aquila, Monteluco di Roio, I-67040 L'Aquila, Italy
        Tel: +39-862-434412, Fax: +39-862-434414, e-mail: franko@ing.univaq.it3

[5] Dipartimento di Elettronica e Informazione, Politecnico di Milano, P.zza L. Da Vinci 32, 20133 Milano, Italy.
        Tel.: +39-02-23993586, Fax.: +39-02-23993413, e-mail: riva@elet.polimi.it

[6] University of Oulu Telecommunication Lab., P.O.Box 444, FIN-90571 Oulu, Finland
        Tel: +358 40 524 2406, Fax: +358-8-553 2845, e-mail: Erkki.Salonen@ee.oulu.fi

2.3 Scintillation/Dynamics of the Signal

Tropospheric scintillation is caused by small-scale refractive index inhomogeneities induced by tropospheric turbulence along the propagation path. It results in rapid fluctuations of received signal amplitude and phase which affect Earth-space links above 10 GHz. On satellite links, the significant scintillation effects are mainly attributed to strong turbulence in clouds and are more severe in summer around noon. Tropospheric scintillation intensity is proved to increase with increasing carrier frequency and with decreasing elevation angle and antenna size. Scintillation fades can have a major impact on the performances of low margin communication systems, for which the long-term availability is sometimes predominantly governed by scintillation effects rather than by rain. In addition, the dynamics of scintillation may interfere with tracking systems or fade mitigation techniques. Scintillation is generally associated with the presence of clouds, especially cumulus and cumulonimbus clouds.

The parameters used for the characterisation of scintillation are the following:

- the amplitude deviation y in dB
- the variance σ^2 and the standard deviation σ of the log-amplitude
- the predicted variance $\sigma_p{}^2$ and standard deviation σ_p

2.3.1 Prediction models for long term standard deviation

All the classical models for scintillation are based on the assumption that the short-term probability density function (pdf) of the log-amplitude is Gaussian. The models are statistical models that allow to calculate either a probability density function or a cumulative distribution function (cdf) of the log-amplitude of the fluctuation or the variance (or standard deviation) of the log-amplitude.

2.3.1.1 Karasawa and ITU-R models

[*Karasawa et al., 1988*] and [*ITU-R, 1999*] present similar prediction models for the calculation of the standard deviation of signal fluctuation due to scintillation. Both these models use the wet part of ground refractivity N_{wet}, a function of relative humidity and temperature, averaged at least over one month, as input parameter.

In the **Karasawa** model, the predicted standard deviation is given by

$$\sigma_p = \sigma_{ref} \sqrt{f^{0.9} G(D_e)/\sin^{2.6}\varepsilon}$$

2.3-1

where

f = frequency [GHz]

ε = link elevation angle

$\sigma_{ref} = 3.42 \times 10^{-3} + 1.186 \times 10^{-4} N_{wet}$

$N_{wet} = \dfrac{22790\, U\, e^{19.7T/(T+273)}}{\left(T+273\right)^2}$ = Air refractivity due to water vapour (wet) at ground level.

U = Relative Humidity at ground level [%].

T = Temperature at ground level [C].

These meteorological input parameters should be averaged over a period of the order of a month.

The factor $G(D_e)$ is an antenna averaging function and its mathematical expression is given by [*Crane and Blood, 1979*]:

$$G(D_e) = \begin{cases} 1.0 - 0.7\left(\dfrac{D_e}{\sqrt{\lambda L}}\right) & for\ 0 \leq \dfrac{D_e}{\sqrt{\lambda L}} \leq 1.0 \\ 0.5 - 0.2\left(\dfrac{D_e}{\sqrt{\lambda L}}\right) & for\ 1.0 < \dfrac{D_e}{\sqrt{\lambda L}} \leq 2.0 \\ 0.1 & for\ 2.0 < \dfrac{D_e}{\sqrt{\lambda L}} \end{cases}$$

2.3-2

where:

λ = wavelength [m]

$D_e = \sqrt{\eta}D$ = Effective antenna diameter [m].

D = Antenna Diameter [m]

η = antenna efficiency

$L = 2h \left/ \left(\sqrt{\sin^2 \varepsilon + 2h/a_e} + \sin \varepsilon\right)\right.$ = distance of the turbulent layer from the receiver [m].

a_e = Effective radius of the earth, including refraction, which is dependent on the station height and is equal to 8.5×10^6 [m] at sea level

h = height of the turbulence. A value of 2000 [m] is suggested by Karasawa.

The model of **ITU-R** [*ITU-R, 1999*] is very similar to the Karasawa model and gives the predicted scintillation variance as:

$$\sigma_p = \sigma_{ref} \sqrt{f^{7/6} g^2(x)/\sin^{2.4} \varepsilon}$$

2.3-3

where:

$\sigma_{ref} = 3.6 \times 10^{-3} + 10^{-4} N_{wet}$

$g^2(x) = 3.8637(x^2 + 1)^{11/12} \sin\left(\dfrac{11}{6} \arctan \dfrac{1}{x}\right) - 7.0835\, x^{5/6}$ = Antenna averaging function by [*Haddon and Vilar, 1986*].

Note that $g^2(x) \approx 1 - 7.0835\, x^{5/6}$ *for* $x << 1$

$x = 0.0584 k D_e^2 / L$

$N_{wet} = \dfrac{22810\, U\, e^{17.5T/(T+240.97)}}{(T + 273)^2}$ = Air refractivity due to water vapour (wet) at ground level.

U = Relative Humidity at ground level [%].

T = Temperature at ground level [C].

$L = 2h \left/ \left(\sqrt{\sin^2 \varepsilon + 2h/a_e} + \sin \varepsilon\right)\right.$ = distance of the turbulent layer from the receiver [m].

a_e = Effective radius of the earth, including refraction, which is dependent on the station height and is equal to 8.5×10^6 [m] at sea level

h = height of the turbulence. A value of 1000 [m] is suggested by ITU-R.

All the parameters are averaged values over a period of at least one month. These models are not able to predict short term standard deviations

The model of Karasawa has been validated by comparison with measurements for elevation angles between 4° and 30°, frequencies in the range 7.3 to 14.2 GHz and antenna diameters from 3 to 36.6m. The average N_{wet} varied from 20 to 130 ppm. The ITU-R model is based on measurements with elevation angles in the range from 4 to 32˚, for frequencies between 7 and 14 GHz and for antenna diameters between 3 and 36 m.

An improvement of the ITU-R model, including the sky noise temperature has been proposed by [*Belloul et al.,1998*].

2.3.1.2 *Otung model*

The model of [*Otung, 1996*] is very similar to the ITU-R one. The difference is in the fact that the ITU-R model uses an empirical dependence on the elevation angle and the Otung model makes use of a factor obtained from simplified theoretical expressions. The predicted scintillation variance becomes:

$$\sigma_p = \sigma_{ref} \sqrt{f^{7/6} g^2(x)/\sin^{11/6} \varepsilon} \qquad \text{2.3-4}$$

This recent model has been validated with one-year measurements in the United Kingdom, using the Olympus 20 GHz beacon, with an elevation angle of 28.7˚ and an antenna of 1.2 m diameter [*Otung & Evans, 1995*].

2.3.1.3 *Ortgies models*

These two recent models of [*Ortgies, 1993*] have been derived from the Olympus experiment data and give the monthly mean value of $ln(\sigma^2)$, indicated as m, as a function of the monthly mean of a meteorological parameter which is either the ground temperature, T, or the air refractivity, N_{wet} :

$$m_n = 0.0462\, N_{wet} - 13.45$$
$$m_n = 0.0865\, T - 12.5 \qquad \text{2.3-5}$$

where:

T = temperature (˚C)

N_{wet} = Air refractivity due to water vapour (wet) at ground level

$m = \ln(\sigma^2)$

$m_n = m + \ln\left(\dfrac{(\sin \varepsilon)^{2.4}}{g^2(D_e) f^a} \right)$

$g^2(D_e)$ = Antenna averaging factor.

a=1.21. As determined from the measurements.

The standard deviation of $ln(\sigma^2)$ appears to be independent of the meteorological data and is found, from the experimental data, to be equal to 1.01.

The model has been derived from 30 months of Olympus measurements in Germany, at 12, 20 and 30 GHz and is assumed to be valid for elevation angles ranging from 6.5° to 30°.

2.3.1.4 *Marzano MPSP and DPSP models*

The Direct Physical Statistical Prediction (DPSP) and the Modelled Physical Statistical Prediction (MPSP) models predicts the monthly mean value of the scintillation variance from ground measurements. They are both based on numerical simulations of the scintillation power as received by a ground station using a large database of radio-sounding observations performed in Milan between January 1980 and December 1989, with a spatial vertical resolution of approximately 150m. The physical model behind these simulations is the one developed by [*Tatarski, 1971*], refined for the intermittent turbulence hypothesis developed by [*d'Auria et al., 1993*] and [*Marzano and d'Auria, 1994*].

Like in the temperature version of Ortgies' model, the DPSP model is based on a direct correlation between the monthly average of $\ln(\sigma_\chi^2)$ and the monthly mean ground temperature *T*.

$$m = \ln\left[g^2(D_e)k^{1.166}(\sin \varepsilon)^{-2.4}\right] + m_n \qquad \text{2.3-6}$$

where

$m_n = -15.84 + 0.1235\,T$

T = monthly mean ground temperature [℃].

$k = \dfrac{2\pi}{\lambda}$ = wave number [m^{-1}]

λ = wavelength [m]

$g^2(D_e)$ = Antenna averaging function

The formulation of the MPSP model by [*Peeters et al., 1997*] is derived from the high correlation between the monthly averaged value of the logarithm of the structure constant $\ln(Cn^2)$ and the monthly mean ground temperature *T*:

$$m = \ln\left[g^2(D_e)k^{7/6}(\sin \varepsilon)^{-11/6}\right] + \ln\left(8.45\,h^{11/6}\right) + \ln\left(C_n^2\right) \qquad \text{2.3-7}$$

where:

$\ln\left(C_n^2\right) = -31.87 + 0.0684\,T$

T = monthly mean ground temperature [℃].

$h = 2058 + 94.5\,T$ = Height of turbulent layer [m]

The models have been validated in Italy with Italsat data at 18, 40 and 50 GHz during a one-year period. New models using other meteorological parameters have been recently developed by [*Marzano and D'Auria, 1998*; *Marzano et al., 1999; Marzano & Riva, 1999*] and validated against ITALSAT data.

2.3.1.5 *Van de Kamp Model*

It has been observed several times, that there is a significant correlation between the occurrence of scintillation and the presence of Cumulus clouds along the propagation path. This gives the impression that at least part of the turbulent activity causing scintillation is associated with Cumulus clouds. The parameter N_{wet}, at ground level, is not a good indicator of this kind of turbulence.

[*Tervonen et al., 1998*] showed that the average variation of scintillation intensity over the hours of the day is uncorrelated with N_{wet}, and strongly correlated with the Cumulus cloud cover. Using the Salonen/Uppala cloud model, an improved version of the model published by [*Salonen and Uppala,*

the whole earth from a ECMWF database. "Heavy clouds" are clouds with an integrated water content larger than 0.70 kg/m^2.

[*Van de Kamp et al., 1999b*] incorporated W_{hc} in a new empirical prediction model for σ_n in the following way:

$$\sigma_p = \frac{\sqrt{g^2(D_e)}f^{0.45}}{\sin^{1.3}\varepsilon}0.98\times10^{-4}\left(N_{wet}+Q\right)$$
<div align="right">2.3-8</div>

$$Q = -39.2 + 56\langle W_{hc}\rangle$$
<div align="right">2.3-9</div>

where

$\langle x\rangle$ = long-term (at least annual) average of the parameter x

W_{hc} = average water content of heavy clouds [kg/m^2].

Q is a long-term average parameter and therefore constant for each site, so that all seasonal dependence of σ_p is still represented by N_{wet}.

2.3.1.6   Frequency dependence of scintillation variance

The expression of the long term variance in the Karasawa and ITU-R models is dependent on system parameters as :

$$\sigma^2 \approx f^a g^2(D_e)\sin^b\varepsilon$$
<div align="right">2.3-10</div>

where

f = frequency [GHz]

ε = elevation angle.

a = 7/6 (ITU-R) or 0.9 (Karasawa)

b = -1.2

The aperture averaging function depends on the ratio between the effective antenna diameter D_e and the Fresnel zone size ($\sqrt{2\pi L/k}$), k being the wavenumber ($k = 2\pi/\lambda$) and L the distance of the turbulent layer.

The ratio of the variances σ_1^2 at f_1 and σ_2^2 at f_2, measured at the same site and with a common elevation is given by

$$\frac{\sigma_1^2}{\sigma_2^2} = \frac{g^2(D_e, f_1)}{g^2(D_e, f_2)}\left(\frac{f_1}{f_2}\right)^a$$
<div align="right">2.3-11</div>

A comparison between a large number of sites has been made by [*Van de Kamp et al., 1999a*]. The value of the frequency exponent *a* for the various sites is given in Figure 2.3-1. This dependence shows remarkable differences from site to site. No convincing correlation of this effect could be found with any meteorological or system parameter. A few hypothesis are proposed: either there is a different frequency scaling for "dry" and "wet" scintillation, or the angle-of-arrival fluctuations have a different frequency scaling factor than the amplitude scintillation and both are mixed in the measurements. This has to be further analysed.
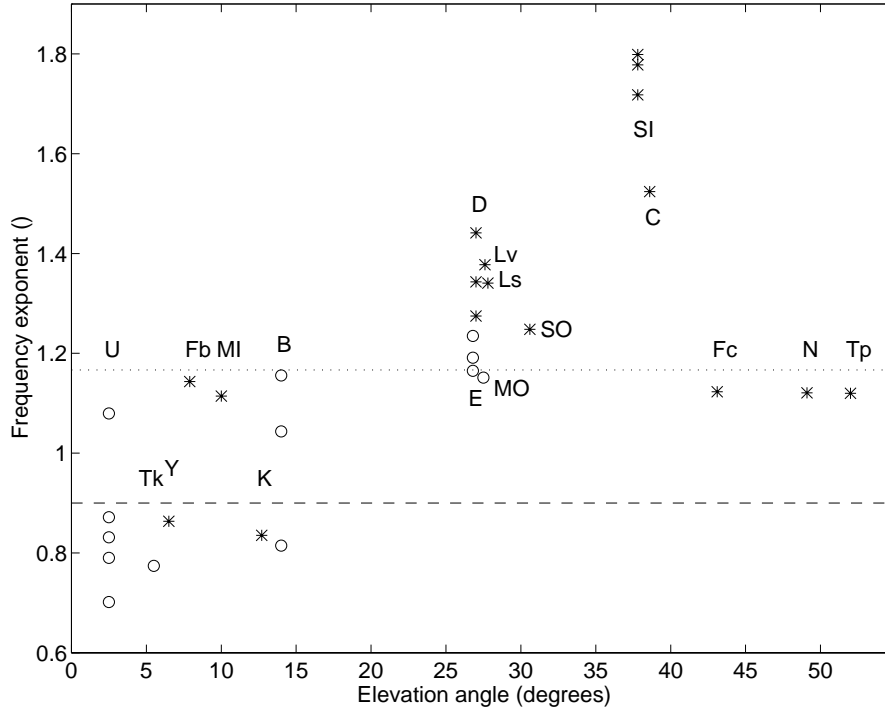
Figure 2.3-1: Frequency exponent a versus elevation angle for all frequency pairs of all measurement sites.
Theoretical relations by ITU-R (……) and Karasawa (----).

2.3.2 Prediction model for cumulative distribution of the log-amplitude and the variance of scintillation

2.3.2.1 Karasawa and ITU-R models

[*Karasawa et al., 1988*] present some expressions for the long-term cumulative distribution of amplitude deviation, expressed in terms of the predicted long-term standard deviation. They derived this expression theoretically, integrating the distribution function of short-term standard deviations, for which they assume a Gamma distribution, with the conditional short-term distribution function of signal level for a given standard deviation, which is generally assumed to be Gaussian. The resulting amplitude deviation y, exceeded for a time percentage P, is:

$$y = \left(-0.0597\log^3 P - 0.0835\log^2 P - 1.258\log P + 2.672\right)\sigma_p \qquad 2.3\text{-}12$$

where:

$0.01\% \leq \mathrm{P} \leq 50\%$.

σ_p is the long-term signal standard deviation (see previous section).

This equation agreed well with the measurements of [*Karasawa et al., 1988*] for signal enhancement. For signal fade however, the measured deviation was larger, especially in the low probability region. They fitted a curve to these measurement results, giving the relation:

$$y = \left(-0.061\log^3 P - 0.072\log^2 P - 1.71\log P + 3.0\right)\sigma_p \qquad 2.3\text{-}13$$

for $0.01\% \leq P \leq 50\%$.

The difference between fade and enhancement is due to an asymmetry in the short-term signal level fluctuations, which is especially evident for strong scintillation. The ITU-R adopted only the distribution for signal fade in their proposed prediction method.

The validity of these methods is the same as the one given in the previous section.

2.3.2.2 Otung Model

[*Otung, 1996*] gives annual and worst month distributions for enhancement and fading. The regression coefficients are extracted from one year measured data at 20 GHz in the UK.

2.3.2.3 Ortgies Model

Assuming that the variance follows a log-normal distribution

$$P\left(\sigma^2\right) = \frac{1}{\sqrt{2\pi}\, s\sigma^2} \exp\left\{ - \frac{\left(\ln \sigma^2 - m\right)^2}{2s^2} \right\}$$

2.3-14

where:

m = the mean value of $\ln\sigma^2$. It can be estimated as described in Section 2.3.1.3

s = the standard deviation of $\ln\sigma^2$. The measured value is 1.01.

2.3.2.4 Van de Kamp Model

The Karasawa model for signal enhancement had been derived assuming a Gaussian short-term distribution of signal level y in dB.

[*Van de Kamp, 1998*] demonstrated that this assumption is not necessarily correct. The main cause of scintillation on a satellite link being turbulence in clouds, this implies that the turbulent layer is likely to be a thin layer far from the receiver. From this modelling approach, it follows that the received electric field amplitude is on a short term Rice-Nakagami distributed, and the distribution of signal level in dB is asymmetrical. This can explain the difference between measured fade and enhancement. The effect of this on the long-term distribution of y is that the normalised fade increases with the long-term standard deviation, while the normalised enhancement decreases. This agrees with the behaviour observed by various authors, which confirms the assumption of the thin turbulent layer and the Rice-Nakagami distribution.

A new model is proposed as

$$y_f(P) = \gamma(P) + \delta(P)$$
$$y_e(P) = \gamma(P) - \delta(P)$$

2.3-15

where

$y_f(P)$ = the distribution of signal fade [dB]

$y_e(P)$ = the distribution of signal enhancement (dB).

The following relationship proposed by [*Van de Kamp, 1998*], is obtained by curve fitting:

$$\gamma(P) = \left(-0.0515 \log^3 P + 0.206 \log^2 P - 1.81 \log P + 2.81\right)\sigma_{lt}$$
$$\delta(P) = \left(0.172 \log^2 P - 0.454 \log P + 0.274\right)\sigma_{lt}^2$$

2.3-16

where

These equations form a new model for the long-term distribution of signal level. The advantages of this model with respect to Karasawa's model are that the asymmetry of the long-term distribution is now theoretically predicted, and this asymmetry increases with the scintillation intensity, consistent with measurement results.

2.3.2.5 *UCL method*

Radiosonde data are a valuable source of information for characterising tropospheric turbulence and a statistical method has been proposed to derive long-term scintillation statistics. The method is described by [*Vasseur et al., 1996*] and [*Vasseur et al., 1998*]. It consists of two main steps.

In the first step, the statistical characteristics of the refractive index structure parameter vertical profile are extracted from radiosonde ascent data collected over a long time period. For this purpose, a statistical model is used to estimate turbulence parameters from meteorological soundings.

In the second step, long-term statistics of slant-path scintillation are derived from the inferred tropospheric turbulence feature, using a rigorous statistical approach and the theory of propagation through a turbulent medium. In addition to radiosonde data, the only parameters required for scintillation prediction are the frequency, elevation angle (the method is valid at elevations higher than about 5 to 10°) and antenna diameter.

The proposed method does not suffer from the limitations of the current empirical scintillation prediction models. It does not include any particular propagation measurement but is only based on radiosonde data and theoretical considerations. The method is applied to one year radiosonde data collected in Belgium and the prediction results compare very well with the scintillation measurements carried out using an Olympus ground station located near to the meteorological station.

2.3.3 References

[*Belloul et al.,1998*]
Belloul B., S. Saunders, B. Evans, "Prediction of Scintillation Intensity from Sky-noise Temperature in Earth-Satellite Links", Electr. Lett., vol. 34, n°10, pp. 1023-1024, 1998.

[*Crane and Blood, 1979*]
Crane R.K. and D.W. Blood, "Handbook for the estimation of microwave propagation effects", NASA Contract NAS5-25341, NASA GSFC Greenbelt, MA, Technical Report No°1, Doc. 7376-TR1, June 1979.

[*d'Auria et al., 1993*]
d'Auria G., F.S. Marzano, U. Merlo, "Model for Estimating the Refractive Index Structure Constant in Clear-Air Intermittent Turbulence", Applied Optics, vol. 32, pp. 2674-2680, 1993.

[*Haddon and Vilar, 1986*]
Haddon J., E. Vilar, "Scattering Induced Microwave Scintillation from Clear Air and Rain on Earth-Space Paths and the Influence of the Antenna Aperture", IEEE Trans. Ant. Prop., vol. 34, No° 5, pp. 646-657, 1986.

[*ITU-R, 1999*]
ITU-R, Rec. PN. 618-6 "Propagation Data and Prediction Methods Required for Earth-Space Telecommunication Systems ", 1999.

[*Karasawa et al., 1988*]
Karasawa Y., M. Yamada, J.E. Allnutt, "A New Predicition Method for Tropospheric Scintillation on Earth-Space Paths", IEEE Trans. Ant. Prop., vol 36, No°11, pp. 1608-1614, 1988.

[*Marzano and d'Auria, 1994*]
Marzano F.S., G. d'Auria, "Estimation of Intermittent Scintillation on Microwave Links from Meteorological Data", Alta Frequenza, vol. 6, pp. 94-97, 1994.

[*Marzano and d'Auria, 1998*]
Marzano F.S., G. d'Auria, "Model-based prediction of amplitude scintillation variance due to clear-air turbulence for Earth-satellite microwave links", IEEE Trans. Ant. Prop., vol. 46, pp. 1506-1518. 1998.

[*Marzano et al., 1999*]
Marzano F. S., C. Riva, A. Banich, F. Clivio, "Assessment of model-based scintillation variance prediction on long-term basis using ITALSAT satellite measurements", Int. J. Sat. Com., vol. 17, Issue 1, pp. 17-36, 1999.

[*Marzano & Riva, 1999*]
Marzano F.S. and C. Riva, "Evidence of long-term correlation between clear-air scintillation and attenuation in microwave and millimeter-wave satellite links", IEEE Trans. Ant. Prop., vol. 47, pp. 1749-1757, 1999.

[*Ortgies, 1993*]
Ortgies G., "Prediction of Slant-Path Amplitude Scintillations from Meteorological Parameters", Proc. 1993 Int. Symp. Radio Propagation, Beijing, pp. 218-221, 1993.

[*Otung, 1996*]
Otung I. E., Prediction of Tropospheric Amplitude Scintillation on a Satellite Link", IEEE Trans. Ant. Prop., vol. 44, n°12, pp. 1600-1608, 1996.

[*Otung & Evans, 1995*]
Otung I.E., B.G. Evans, "Short Term Distribution of Amplitude Scintillation on a Satellite Link",

[*Peeters et al., 1997*]
Peeters G., F.S. Marzano, G. d'Auria, C. Riva, D. Vanhoenacker-Janvier, "Evaluation of Statistical Models for Clear-Air Scintillation Using Olympus Satellite Measurements", Int. J. Sat. Com., vol. 15, pp. 73-88, 1997.

[*Salonen et al., 1994*]
Salonen E., S. Karhu, S. Uppala and R. Hyvönen, "Study of improved propagation predictions", Final Report for ESA/Estec Contract 9455/91/NL/LC(SC), Helsinki University of Technology and Finnish Meteorological Institute, pp. 83-87, 1994.

[*Salonen and Uppala, 1991*]
Salonen E. and S. Uppala, "New prediction method of cloud attenuation", Electr. Lett., vol. 27, pp. 1106-1108, 1991.

[*Tatarski, 1971*]
Tatarski V.I., "The effects of the turbulent atmosphere on Wave Propagation", Israel Program for Scientific Translations, Jerusalem, 1971.

[*Tervonen et al., 1998*]
Tervonen J. K, M.M.J.L. van de Kamp and E. T. Salonen, "Prediction Model for the Diurnal Behavior of the Tropospheric Scintillation Variance", IEEE Trans. Ant. Prop., vol. 46, pp. 1372-1378, 1998.

[*Van de Kamp, 1998*]
Van de Kamp M.M.J.L., "Asymmetrical signal level distribution due to tropospheric scintillation", Electr. Lett, vol. 34, pp. 1145-1146, 1998.

[*Van de Kamp et al., 1999a*]
Van de Kamp M.M.J.L., C. Riva, J. Tervonen, E. Salonen, "Frequency Dependence of Amplitude Scintillation", IEEE Trans. Ant. Prop., vol. 47, No°1, pp. 77-85, 1999.

[*Van de Kamp et al., 1999b*]
Van de Kamp M.M.J.L., J.K. Tervonen, E.T. Salonen, and J.P.V. Poiares Baptista, "Improved Models for Long-Term Prediction of Tropospheric Scintillation on Slant Paths", IEEE Trans. Ant. Prop., vol. 47, n°2, pp. 249-260, 1999.

[*Vasseur et al., 1996*]
Vasseur H., O. Ravard, D. Vanhoenacker-Janvier, "Prediction of slant-path scintillation from radiosonde measurements", Proc. Climpara'96, pp. 12-13, Oslo, June 1996.

[*Vasseur et al., 1998*]
Vasseur H., D. Vanhoenacker, "Characterisation of tropospheric turbulent layers from the radiosonde data", Electr. Lett., vol. 34, No°4, pp. 318-319, 1998.

CHAPTER 2.4
Rain and Ice Depolarisation

Editor: Antonio Martellucci[1]

Authors: Max van de Kamp[2], Antonio Martellucci[1], Aldo Paraboni[3]

[1] European Space Agency, Estec, Keplerlaan 1, Postbus 299, 2200 AG Noordwijk, The Netherlands
Tel: +31 71 565 5603, Fax: +31 71 565 4999, e-mail: Antonio.Martellucci@esa.int

2 Eindhoven University of Technology, Postbus 513, 5600 MB Eindhoven, The Netherlands
Tel.: +31 40 247 2326, Fax.: +31 40 245 5197, e-mail: m.m.j.l.v.d.kamp@ele.tue.nl

3 Politecnico di Milano, CSTS, Pza Leonardo da Vinci 32, 20133 Milano, Italy
Tel. +39 2 23993586, Fax +39 2 3993413, e-mail: aparaboni@elet.polimi.it

2.4 Rain and Ice Depolarisation

The development of radio communication systems making use of wave polarisation in the 20/30 and 40/50 GHz frequency bands requires an accurate modelling of the atmospheric transfer matrix. The polarisation of the electromagnetic wave propagating in the atmosphere can be modified by the presence in the atmosphere of non-spherical particles such as raindrops and ice crystals. Rain and ice contribute in a different way to depolarisation, depending on the frequency band, the contribution of ice being more relevant as the frequency increases.

The full characterisation of the depolarising medium can be obtained by means of the atmospheric transfer matrix. The transfer matrix can be completely described, under general assumptions, using "*anisotropy*" and "*canting angle*". As discussed in the following, these parameters are strictly related to the physical mechanisms producing depolarisation (inclined hydrometeors axis, wind shear, turbulence, etc), can be scaled in frequency and can be predicted using climatological parameters. Furthermore the ice and rain depolarisation can be assessed separately and combined on a physical basis. The "quasi-physical" parameters can either be calculated theoretically or derived from the statistical database of the measurements performed in the framework of the Olympus and Italsat propagation experiments.

The transfer matrix modelling permits to define the joint statistical distribution of depolarisation and rain attenuation (including also ice effects in the absence of rain) that is particularly required for the estimation of digital system performances.

A simpler approach, based on the average relationship between rain attenuation and cross-polar discrimination (XPD) like the one used by the ITU_R model [*ITU-R, 1999*], is practical, as an alternative to the transfer matrix description, when only the atmospheric XPD needs to be estimated. During the COST 255 project, the current model of ITU-R for crosspolar-discrimination has been extended up to V-Band.

Nevertheless the comparison of these models with Olympus and Italsat propagation measurements in the Ka- and V-Bands (see Chapter 2.6) has demonstrated that they can underestimate the worst cases of ice depolarisation in absence of rain or during moderate rainfalls.

The appendix contains a brief review of of polarisation, intended to simplify conversion between the different methods used to describe the polarisation of an electromagnetic wave.

2.4.1 Definition of the atmospheric transmission matrix

The effect of the atmosphere on the electromagnetic wave can be described by means of the transfer matrix **T** [*Capsoni and Paraboni, 1972*], [*Oguchi, 1983*].

The matrix **T** relates the input electric field, $\mathbf{E}_T$, to that received, $\mathbf{E}_R$:

$$\begin{bmatrix} E_{xr} \\ E_{yr} \end{bmatrix} = \begin{bmatrix} T_{xx} & T_{xy} \\ T_{yx} & T_{yy} \end{bmatrix} \cdot \begin{bmatrix} E_{xt} \\ E_{yt} \end{bmatrix}$$

2.4-1

where

$\begin{bmatrix} E_{xi} \\ E_{yi} \end{bmatrix} \equiv \mathbf{E}_i$ = amplitude of the transmitted/received (i = T or R) electric field along the x and y axes

$$\mathbf{T} \equiv \begin{bmatrix} T_{xx} & T_{xy} \\ T_{yx} & T_{yy} \end{bmatrix} = \text{atmospheric transfer matrix using } \mathbf{x} \text{ and } \mathbf{y} \text{ polarisations}$$

T_{ij} = copolar component received on the channel employing polarisation i, when an electric field with an amplitude equal to one is transmitted on the channel employing polarisation j. (i and $j = x$ or y).

When two generic orthogonal polarisations, $E_{//}$ and $E_{\perp}$, are transmitted, the transfer matrix, $\mathbf{T}$, can be transformed into the matrix $\mathbf{M}$, by using:

$$\mathbf{M} = \begin{bmatrix} \cos(\alpha) & e^{-j\delta}\sin(\alpha) \\ \sin(\alpha) & -e^{-j\delta}\cos(\alpha) \end{bmatrix} \cdot \mathbf{T} \cdot \begin{bmatrix} \cos(\alpha) & \sin(\alpha) \\ e^{+j\delta}\sin(\alpha) & -e^{+j\delta}\cos(\alpha) \end{bmatrix} \qquad 2.4-2$$

where:

$$E_{//} = E_0 \left[\cos(\alpha)\mathbf{x} + \sin(\alpha)e^{j\delta}\mathbf{y} \right]$$

α, δ = Parameters that describes the transmitted polarisation. (See Section 1 of the appendix).

A particular case of $\mathbf{M}$ occurs when circular polarisation is employed. The transfer matrix, $\mathbf{C}$, expressed using the right, r, and left-hand, l, circular polarisation, E_r and E_l is:

$$\begin{bmatrix} E_{rr} \\ E_{lr} \end{bmatrix} = \begin{bmatrix} C_{rr} & C_{rl} \\ C_{lr} & C_{ll} \end{bmatrix} \cdot \begin{bmatrix} E_{rt} \\ E_{lt} \end{bmatrix} \qquad 2.4-3$$

where:

$$\mathbf{C} \equiv \begin{bmatrix} C_{rr} & C_{rl} \\ C_{lr} & C_{ll} \end{bmatrix} = \text{Atmospheric transfer matrix using right and left hand circular polarisation}$$

$$C_{rr} = ? \left[(T_{xx} + T_{yy}) + j(T_{yx} - T_{xy}) \right] \; ; \; C_{ll} = ? \left[(T_{xx} + T_{yy}) - j(T_{yx} - T_{xy}) \right]$$

$$C_{rl} = ? \left[(T_{xx} - T_{yy}) + j(T_{yx} + T_{xy}) \right] \; ; \; C_{lr} = ? \left[(T_{xx} - T_{yy}) - j(T_{yx} + T_{xy}) \right]$$

The copolar term of the transfer matrix, T_{ii}, describes the fading of polarisation i, A_i, in dB:

$$\begin{array}{ll} A_x = -20\log(T_{xx}) & A_{cr} = -20\log(C_{rr}) \\ A_y = -20\log(T_{yy}) & A_{cl} = -20\log(C_{ll}) \end{array} \qquad 2.4-4$$

The crosspolar discrimination, XPD_{ij}, is the ratio between the copolar component received on the channel employing polarisation j, T_{jj}, and the crosspolar component received on the channel using polarisation i, T_{ij}, when only polarisation j is transmitted:

$$\begin{array}{ll} XPD_{xy} = 20\log\left|T_{yy}/T_{xy}\right| & XPD_{rl} = 20\log\left|C_{ll}/C_{rl}\right| \\ XPD_{yx} = 20\log\left|T_{xx}/T_{yx}\right| & XPD_{lr} = 20\log\left|C_{rr}/C_{lr}\right| \end{array} \qquad 2.4-5$$

where :

$T_{ij}/T_{jj} = \rho_{ij} = $ complex depolarisation ratio

The crosspolar isolation, XPI_{ij}, is defined as the ratio between the copolar part of the signal on the channel using polarisation i, T_{ii}, and the crosspolar component of the signal received on the same

$$XPI_{xy} = 20\log|T_{xx}/T_{xy}| \quad ; \quad XPI_{xy} = 20\log|T_{xx}/T_{xy}|$$
$$XPI_{yx} = 20\log|T_{yy}/T_{yx}| \quad , \quad XPI_{yx} = 20\log|T_{yy}/T_{yx}|$$

$$\text{2.4-6}$$

The transfer matrix T can be normalised to one of its elements, e.g. T_{xx}. Therefore only a maximum of three complex parameters is actually needed to describe the transfer channel.

The two eigenvectors of the transfer matrix **T,** defined as the **characteristic polarisations**, represent the two polarisations that propagate in the atmosphere without undergoing depolarisation [*Capsoni and Paraboni, 1972*; *Oguchi, 1983*].

If the characteristic polarisations are linear, then they are orthogonal vectors and the planes identified by the linear polarisation vectors and the propagation direction are defined as **principal planes** of the transfer channel.

In the general case, the eigenvalues of the transfer matrix **T** are related to the propagation constants of the characteristic polarisations and are given by:

$$\Gamma_I = \exp(-\gamma_I) = \frac{1}{2}\left[(T_{yy} + T_{xx}) + \sqrt{(T_{yy} - T_{xx})^2 + 4T_{xy}T_{yx}}\right]$$
$$\Gamma_{II} = \exp(-\gamma_{II}) = \frac{1}{2}\left[(T_{yy} + T_{xx}) - \sqrt{(T_{yy} - T_{xx})^2 + 4T_{xy}T_{yx}}\right]$$

$$\text{2.4-7}$$

where:

γ_I , γ_{II} = propagation constants of the eigenvectors I e II, defined as characteristic polarisations.

I = Polarisation characterised by the lower attenuation or the lower phase shift.

II = Polarisation characterised by the higher attenuation or the higher phase shift.

The anisotropy of the medium, Δ, is defined as the difference between the propagation constants of the characteristic polarisations:

$$\Delta = \gamma_{II} - \gamma_I \qquad \text{2.4-8}$$

where:

Re(Δ) = Differential Attenuation of the atmosphere for the characteristic polarisations, [nep]

Im(Δ) = Differential phase shift of the atmosphere for the characteristic polarisations, [rad]

In the general case, the eigenvectors of characteristic polarisations, **E**$_I$ and **E**$_{II}$, of the transfer matrix T are elliptical polarisations and are given by:

$$\mathbf{E}_I = \begin{pmatrix} (T_{yy} - T_{xx}) + \sqrt{(T_{yy} - T_{xx})^2 + 4T_{xy}T_{yx}} \\ -2T_{xy} \end{pmatrix} \quad ; \quad \mathbf{E}_{II} = \begin{pmatrix} 2T_{xy} \\ (T_{yy} - T_{xx}) + \sqrt{(T_{yy} - T_{xx})^2 + 4T_{xy}T_{yx}} \end{pmatrix}$$

$$\text{2.4-9}$$

where:

$\mathbf{E}_I \cdot \mathbf{E}_{II} = 0$

The two characteristic polarisations can be described by means of the complex canting angle of eigenvector II, Φ (see Section 6 of the appendix), that is given by the following relationship:

$$\tan(\Phi) = \frac{(T_{yy} - T_{xx}) + \sqrt{(T_{yy} - T_{xx})^2 + 4T_{xy}T_{yx}}}{2T_{xy}} \qquad \text{2.4-10}$$

where:

$\mathrm{Re}(\Phi)$ = Canting angle of the ellipse with respect x axes. $-\pi/2 < \mathrm{Re}(\Phi) \leq +\pi/2$

$\tanh[\mathrm{Im}(\Phi)]$ = Axial ratio of the ellipse.

The occurrence of principal planes in the atmospheric medium is revealed by the condition, $\mathrm{Im}\{\Phi\} = 0$. In this particular case the characteristic polarisations, E_I and E_{II}, are two orthogonal linear polarisations, canted at an angle $\mathrm{Re}\{\Phi\}$ with respect to the y and x axes.

2.4.2   Model of the transfer matrix

A model of the propagation of a polarised electromagnetic plane wave through a spatial distribution of non-spherical particles, can be derived under the following general assumptions:

1) The amplitude of the field scattered by the particles can be calculated using the Fresnel approximation.

2) The contribution to the transmitted field by scattering from directions different from the propagation direction of the plane wave can be ignored. (i.e. only the forward scattering by particles contributes to the transmitted field).

3) The shape of atmospheric particles (rain drops and ice crystals) has an axis of symmetry.

4) The distribution of particles is longitudinally homogeneous.

Using these assumptions the differential equation that describes the electromagnetic wave propagation can be solved, by means of the technique based on eigenvectors and eigenvalues [*Capsoni et al., 1981*]. It turns out that the number of complex parameters, needed to describe the transfer matrix T, reduces from three to two. The medium transfer matrix, using linear polarisations x and y, is given by:

$$T = \exp\left(-l\frac{\gamma_x + \gamma_y}{2}\right) \cdot \left[\cosh\left(\frac{\Delta}{2}\right)\cdot\begin{pmatrix}1 & 0 \\ 0 & 1\end{pmatrix} - \sinh\left(\frac{\Delta}{2}\right)\cdot\begin{pmatrix}\cos(2\Phi) & \sin(2\Phi) \\ \sin(2\Phi) & -\cos(2\Phi)\end{pmatrix}\right] \qquad 2.4\text{-}11$$

where :

γ_x, γ_y =   propagation constants of x and y polarisations

$\Delta = \gamma_{II} - \gamma_I$ =   anisotropy of the medium.

γ_I, γ_{II} =   propagation constants of characteristic polarisations I and II.

$\Phi = \Phi_R + j\Phi_I$ =   complex canting angle of polarisation II

l   =   length of dispersion of particles.

Therefore the transfer matrix can be completely described by means of the **anisotropy of the medium**, Δ, and the **complex canting angle**, Φ.

The crosspolar discrimination of linear polarisation can be calculated using the complex depolarisation ratios (see equation 2.4-5):

$$\rho_{xy} = \frac{-\tanh\left(\frac{\Delta}{2}\right)sen(2\Phi)}{1 + \tanh\left(\frac{\Delta}{2}\right)\cos(2\Phi)} \quad ; \quad \rho_{yx} = \frac{-\tanh\left(\frac{\Delta}{2}\right)sen(2\Phi)}{1 - \tanh\left(\frac{\Delta}{2}\right)\cos(2\Phi)} \qquad 2.4\text{-}12$$

The medium transfer matrix **C**, when right or left handed circular polarisation are transmitted, is given by:

$$C = \exp\left(-l\frac{\gamma_x + \gamma_y}{2}\right) \cdot \left[\cosh\left(\frac{\Delta}{2}\right) \cdot \begin{pmatrix} 1 & 0 \\ 0 & 1 \end{pmatrix} - \sinh\left(\frac{\Delta}{2}\right) \cdot \begin{pmatrix} 0 & \exp(+j2\Phi) \\ \exp(-j2\Phi) & 0 \end{pmatrix}\right]$$

2.4-13

Similarly the complex depolarisation ratios of circular polarisation are:

$$\rho_{rl} = -\tanh\left(\frac{\Delta}{2}\right)\exp(j2\Phi) \; ; \quad \rho_{lr} = -\tanh\left(\frac{\Delta}{2}\right)\exp(-j2\Phi)$$

2.4-14

The propagation parameters needed for the evaluation of the atmospheric transmission matrix can be calculated using the scattering matrix of all the particles:

$$\gamma_x = jk + \frac{2\pi}{k^2}\sum S_{xx}(f,a,\theta,\phi)$$

$$\gamma_y = jk + \frac{2\pi}{k^2}\sum S_{yy}(f,a,\theta,\phi)$$

2.4-15

$$\Delta = \frac{2\pi}{k^2}\sqrt{\sum (S_2 - S_1)\exp(+2j\phi)\sum (S_2 - S_1)\exp(-2j\phi)}$$

$$\Phi = \frac{j}{4}\ln\left[\frac{\sum (S_2 - S_1)\exp(-2j\phi)}{\sum (S_2 - S_1)\exp(+2j\phi)}\right]$$

2.4-16

where:

the sum is performed over all the particles contained in the distribution

f = frequency [Hz]

a = parameter that describes the dimension of the particle (e.g. equivolumetric radius).

θ, ϕ = angles that describe the spatial orientation of the symmetry axis of each particle, with respect to the propagation direction, on longitudinal plane ($\theta, \; 0 < \theta \leq \pi$) and transverse plane ($\phi, \; -\pi/2 < \phi \leq +\pi/2$)

k = $2\pi/\lambda$ = wave-number [rad/m]

S_1, S_2 = copolar elements of the scattering matrix when polarisation 1 or 2 are transmitted.

Polarisations 1 or 2 are respectively parallel and orthogonal to the symmetry axis of the particle.

$$\left.\begin{array}{l} S_{xx} = (S_1 + S_2)/2 + \cos(2\phi)(S_2 - S_1)/2 \\ S_{yy} = (S_1 + S_2)/2 - \cos(2\phi)(S_2 - S_1)/2 \\ S_{xy} = S_{yx} = \sin(2\phi)(S_2 - S_1)/2 \end{array}\right\}$$ = Elements of the particle scattering matrix (x or y polar[n]).

For a general description of models to calculate the scattering matrix see [*Poiares Baptista, 1994*].

From the previous equations it can be derived that the characteristic polarisations are linear and the medium is characterised by the existence of principal planes of polarisation (i.e. Im(Φ)=0) when one of the following conditions holds:

1) The scattering matrix of the particles can be calculated using the Rayleigh approximation for spheroidal particles.

2) The statistical distribution of the orientations of the particle symmetry axis is a symmetric function.

This general model can be further developed to describe the following particular cases:

2.4.2.1 Fully aligned particles

When all the particles are aligned, with their symmetry axes oriented along the direction described by the longitudinal canting angle θ_o and the transverse canting angle ϕ_o, the total anisotropy and the complex canting angle of the medium are given by the following relationships:

$$\Delta = \frac{2\pi}{k} l \int n(a)[S_2(f,a,\theta_0,\phi_0) - S_2(f,a,\theta_0,\phi_0)]da \qquad \text{2.4-17}$$

$$\mathrm{Re}(\Phi) = \phi_0 \;; \; \mathrm{Im}(\Phi) = 0 \qquad \text{2.4-18}$$

where:

$n(a)$ = distribution of drop size.

l = length of dispersion of particles.

Therefore the characteristic polarisations are linear and canted at an angle ϕ_0 with respect to the x and y axes.

2.4.2.2 Particles with Gaussian distribution of orientations

When the longitudinal canting angle θ and the transverse canting angle ϕ are statistically independent and are distributed according to a normal model, the total anisotropy and the complex canting angle of the medium are given by the following relationships:

$$\Delta = r\frac{2\pi L}{k^2} \int n(a)[S_2(f,a,\theta_0,\phi_0) - S_1(f,a,\theta_0,\phi_0)]da \qquad \text{2.4-19}$$

$$\mathrm{Re}(\Phi) = \phi_0 \;; \; \mathrm{Im}(\Phi) = 0 \qquad \text{2.4-20}$$

where:

$r = \frac{1}{2}[1 + \exp(-2\sigma_\theta^2)]\exp(-2\sigma_\phi^2) = $ reduction factor of the anisotropy due to misalignment of particles

θ_o, ϕ_o = mean values of longitudinal and transverse canting angle.

$\sigma_\theta, \sigma_\phi$ = standard deviations of longitudinal and transverse canting angle.

Therefore the medium is still characterised by linear characteristic polarisations and equation 2.4-17 can be used by taking into account the reduction factor r.

2.4.2.3 Medium composed of two different types of particle

It is assumed that in the atmosphere there are two different distributions of particles in cascade, e.g. rain and ice. Each family is characterised by anisotropy, Δ_1 and Δ_2, and the characteristic polarisations are linear, canted at angles ϕ_1 and ϕ_2 with respect to the x and y axes [*Martellucci et al., 1993; Martelluci & Paraboni, 1994; Dintelmann, 1994*].

The overall transmission matrix **T** is the product of the two transmission matrices **T**₁ and **T**₂. The

$$\tanh(\Delta/2) \cong \Delta/2 \qquad \text{and that} \qquad T_{xx1}T_{xx2} + T_{xy1}T_{yx2} \cong T_{xx1}T_{xx2}.$$

Using these approximations the overall transfer matrix of the atmosphere, using circular polarisation, is given by :

$$\mathbf{C} = \begin{bmatrix} 1 & C_{rl} \\ C_{lr} & 1 \end{bmatrix} \qquad\qquad 2.4\text{-}21$$

where:

$$C_{rl} = -\frac{d_1}{2}\exp[j(\alpha_1 + 2\phi_1)] - \frac{d_2}{2}\exp[j(\alpha_2 + 2\phi_2)]$$

$$C_{lr} = -\frac{d_1}{2}\exp[j(\alpha_1 - 2\phi_1)] - \frac{d_2}{2}\exp[j(\alpha_2 - 2\phi_2)]$$

$\Delta_i = d_i \exp(j\alpha_i) = \quad$ anisotropy of the first or second (i=1 or 2) family of particles.

$d_i \qquad\qquad = \quad$ amplitude of anisotropy of family i

$\alpha_i \qquad\qquad = \quad$ phase of anisotropy of family i.

$\phi_1, \phi_2 \qquad\quad = \quad$ canting angle of the linear characteristic polarisation of the first and the second families of particles.

The overall anisotropy of the medium, Δ, can be obtained by inversion of equation 2.4-13:

$$\Delta = \sqrt{K_1 + K_2 + K_3} \equiv 2\sqrt{C_{rl}C_{lr}} \qquad\qquad 2.4\text{-}22$$

where:

$$K_1 = d_1^2 \exp(j2\alpha_1)$$

$$K_2 = d_2^2 \exp(j2\alpha_2)$$

$$K_3 = 2d_1 d_2 \cdot \exp[j(\alpha_1 + \alpha_2)] \cdot \cos[2(\phi_1 - \phi_2)]$$

It is to be noted that by means of anisotropy the difference between the canting angles of the two populations, (ϕ_1 - ϕ_2), also affects the depolarisation. When the two populations are aligned or are geometrically orthogonal, the overall anisotropy becomes:

$$\Delta = \begin{cases} \Delta_1 + \Delta_2 \; ; & \text{for } (\phi_1 - \phi_2) = 0 \\ \Delta_1 - \Delta_2 \; ; & \text{for } (\phi_1 - \phi_2) = \pm \pi/2 \end{cases} \qquad\qquad 2.4\text{-}23$$

Therefore the combination of the depolarisation effects of rain and ice must take into account their relative geometrical orientation, in order to assess if the overall depolarisation is increased or reduced with respect to the separate depolarisations. This is particularly relevant during thunderstorms and at V-Band where the ice depolarisation is higher than at K-Band.

Measurements of Anisotropy and Canting Angle

The model of the atmospheric transfer matrix described in this chapter makes possible the complete assessment of atmospheric depolarisation if the anisotropy and the canting angle are known. The experimental assessment of those parameters has been performed using the dual polarisation propagation beacons of the Olympus and Italsat satellites, at 29,7 and 49.5 GHz respectively [*Dintelmann, 1994*; *Aresu et al. 1994*; *Martellucci et al., 2000*]. Those measurements can be used to

The data measured by the Olympus station located in Spino D'Adda, near Milano, are presented as an example of anisotropy and canting angle on slant paths [*Aresu et al., 1995*]. The elevation to the satellite was 31 degrees and the polarisation tilt angle was 25 degrees.

The presence of ice at low attenuation values has been shown statistically by the Imaginary part of the overall anisotropy, Δ.

In Figure 2.4-1a the statistics are given of the real part of rain anisotropy, conditioned on attenuation. This parameter appears to be linearly related to the rain attenuation. The difference between the theoretical (discussed in Section 2.4.2.4) and the experimental values of the real part of rain anisotropy, suggest a reduction factor of about 0.6, that is in agreement with previous measurements on terrestrial path [*Aresu et al., 1993*].

The anisotropy of ice, conditioned on attenuation, is given in Figure 2.4-1b. The theoretical maximum value of ice anisotropy derived from local radiosonde meteorological measurements is also plotted (see Section 2.4.2.4) [*Paraboni et al., 1997*]. The model value of ice cloud anisotropy is in agreement with the mean value of measurements for attenuation values lower than 20 dB. At higher attenuations the ice anisotropy can be relevant and exhibits a correlation with the intensity of rainfall.
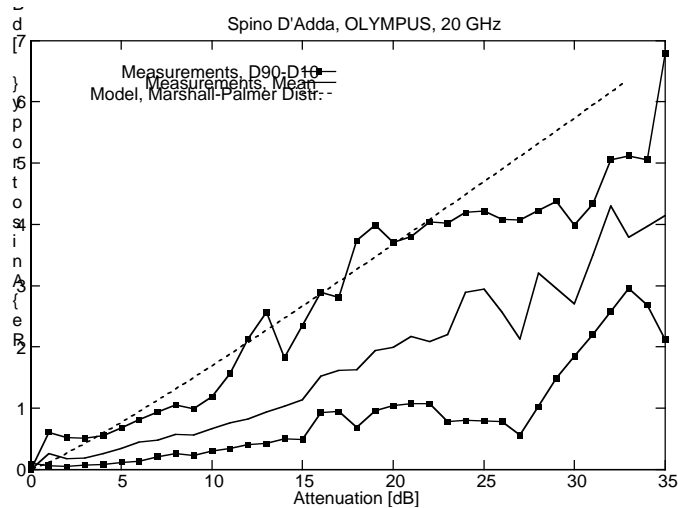

a)
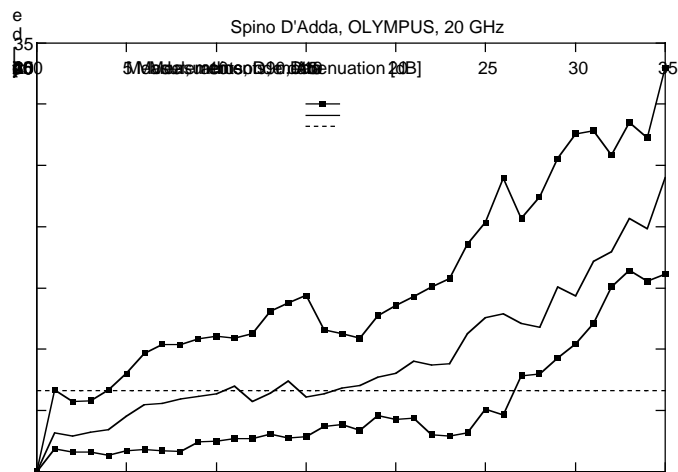
b)

Figure 2.4-1: Deciles of real part of rain anisotropy (a) and imaginary part of ice anisotropy (b)

Italsat measurements of the atmospheric transfer matrix at 49.5 GHz, performed by [*Martellucci et al., 2000*] confirmed the Olympus results. In addition it was found that ice anisotropy at 49.5 GHz can be described by a log-normal model. The average of ice anisotropy value increases with rainfall intensity, and the standard deviation oscillates around a constant value for attenuation values ranging from 0 to 10 dB at 49.5 GHz, then it decreases for higher attenuation values.

The statistics of canting angle, with respect to local horizontal, of the raindrops and ice crystals, conditioned on attenuation values, are given in Figure 2.4-2.

As far as the rain population is concerned, there is a tendency for rain drops to stabilise during thunderstorms within a range of about 20 degrees around the horizontal, confirming similar results obtained on a terrestrial link [*Aresu et al., 1993*].

On the contrary the measurements show that ice crystals can change orientation during thunderstorms, due to electrostatic discharges and aerodynamic effects, leading to fluctuations of more than 50°.
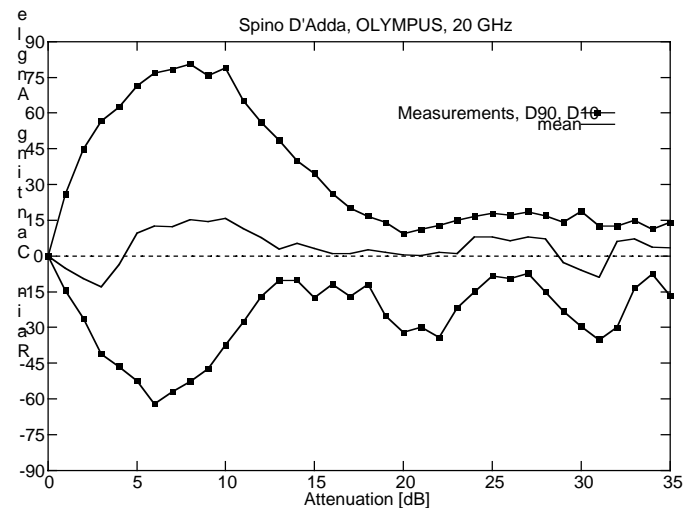
a)
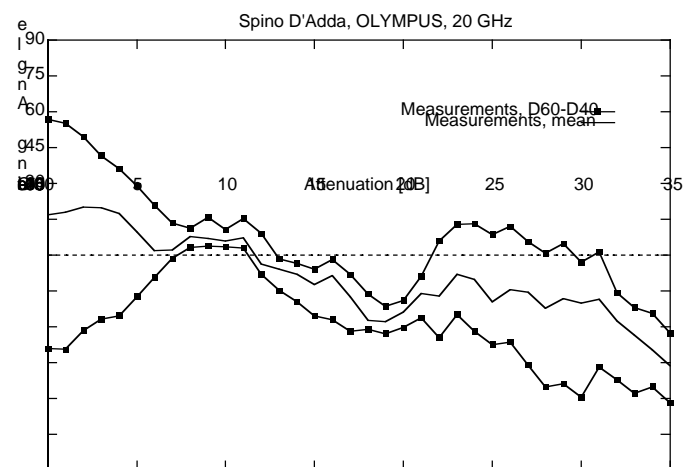
b)

Figure2.4-2: Deciles of canting angle of rain (a) and ice (b) conditioned on attenuation measured in Spino D'Adda, using the Olympus Satellite beacon at 19.77 GHz.

2.4.2.4   Theoretical calculation of depolarisation due to rain and ice

The atmospheric particles that can contribute to microwave depolarisation along a slant path are raindrops, melting particles (formed by a mixture of air, water and ice) and ice crystals. According to the model illustrated in the previous chapter, the depolarisation due to atmospheric particles can be estimated theoretically, by using the appropriate microphysical parameters and models of the atmospheric particles.

As far as the melting layer is concerned, it can be expected that its thickness is lower than the characteristic size of both the ice layer and the rain cell. Therefore the depolarisation of the melting layer can be neglected, as a first approximation, when comparing the rain and ice anisotropy.

In following paragraphs, examples of modelling and calculations of the crosspolar discrimination due to rain and ice clouds in the Ka and V-Bands will be illustrated. The simultaneous occurrence of rain and ice depolarisation is also discussed and a statistical model is presented for estimating the total ice content based on the rain rate at the ground.

The parameters used for those assessments have been derived from analysis of the Olympus and Italsat propagation experiments.

Rain depolarisation

The following parameters and models have been selected for rain depolarisation:

- Water temperature = 0 ˚C.
- Shape of drops = oblate spheroid.
- Orientation of particle symmetry axis = parallel to the vertical direction.
- Model of rain drop size distribution = Marshall-Palmer, exponential.
- Drops are aligned , with a canting angle ranging from 5° to 45°.
- Rain cell length = 1 km.
- The water refractive index has been calculated according to [*Ray, 1972*].
- The scattering matrix of drops is calculated using the Oguchi's Point Matching Technique [*Oguchi, 1983*].

The model parameters have been verified using results from terrestrial measurements, where no ice or snow is measured, and satellite measurements, separating rain and ice [*Aresu et al., 1993; Aresu et al., 1994* and *Aresu et al., 1995*]. The statistics of canting angle, anisotropy and rain reduction factor have been determined from those measurements.
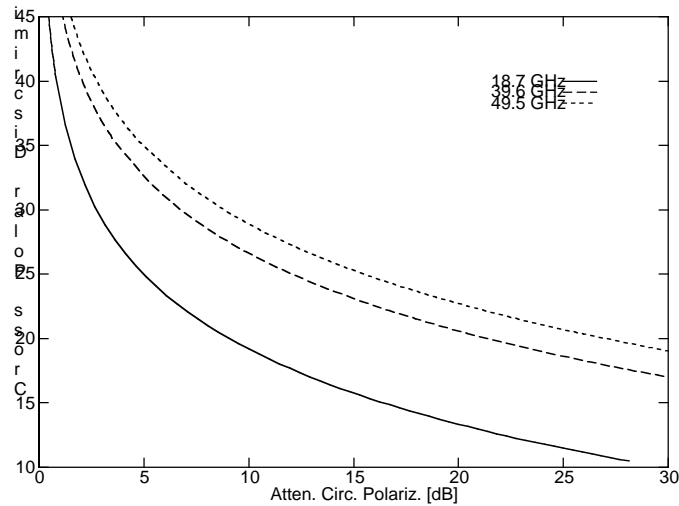
Figure2.4-3: Rain Cross Polar Discrimination of circular polarisation as a function of attenuation at the frequencies of the Italsat propagation beacons. Link elevation = 41°.

The crosspolar discrimination as a function of the attenuation of circular polarisation is independent of the canting angle of the principal planes and is given in Figure 2.4-3. It shows the higher sensitivity of the cross-polar discrimination to the rain attenuation at Ka-Band, with respect to V-Band.

The crosspolar discrimination is lower than 25 dB when the rain attenuation at 18.7, 39.6 or 49.5 GHz is higher than 5, 10 or 15 dB, respectively.

The crosspolar discrimination of linear polarisation is affected by the canting angle of the principal planes, as depicted in Figure 2.4-4. The cross polar discrimination of the linear polarisation along the x axis as a function of attenuation, at 49.5 GHz and for a link elevation of 41°, is plotted for various canting angles of the principal planes. The crosspolar discrimination fluctuates by about 16 dB when the canting angle ranges from 5 to 45 degrees and the attenuation is higher than 16 dB.
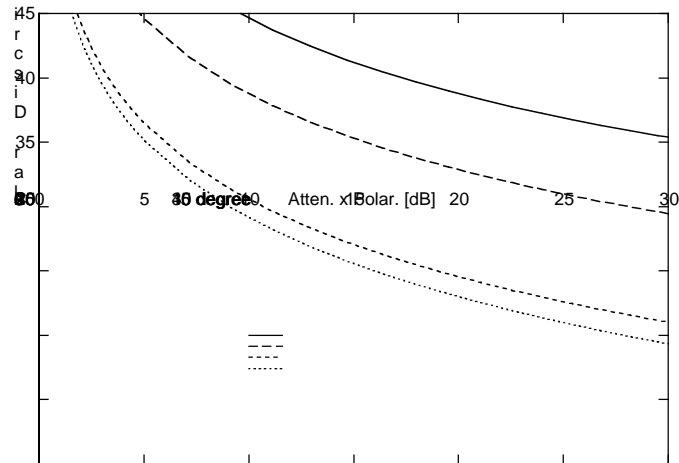

Figure2.4-4: Rain Cross Polar Discrimination of the linear polarisation x, as a function of attenuation, at 49.5 GHz and a link elevation of 41°, for different values of the canting angle of the principal planes

Ice cloud depolarisation

In order to calculate the depolarisation due to ice clouds, the following assumptions and models

- Ice temperature = -15 °C.
- Shape of ice needles = prolate spheroid.
- Model of ice distribution size = Gamma function, Cirrostratus cloud.
- Ice density is assumed to be constant in the vertical direction.
- Scattering functions of ice crystals is calculated using the Rayleigh model.
- The ice refractive index has been calculated according to [*Ray, 1972*].

It can be assumed that the ice needles are maintained aligned on to the horizontal plane by aerodynamic and electrostatic effects, and can rotate freely in this plane.

When the ice crystals are completely aligned, the anisotropy depends on the rotation angle of the crystals and is higher when the rotation angle is equal to 90° and the apparent canting angle is equal to 0°. The apparent canting angle of the ice cloud is given by the projection of the symmetry axes on the plane orthogonal to the direction of propagation:

$$\phi_2(\gamma) = \arctan\left[-\cot(\gamma)\cdot\sin(\theta)\right]$$
<div align="right">2.4-24</div>

where:

γ = Horizontal rotation angle of the symmetry axis of the needle with respect to the propagation direction.

β = elevation angle

When the ice crystals are randomly aligned in to the horizontal plane, the anisotropy is non-zero while the apparent canting angle is equal to zero.

Using this simple model, the ice anisotropy results depend on the total ice content, I:

$$\Delta_i(I) = \Delta_{max}(I)\sqrt{B^2 + C^2}$$
<div align="right">2.4-25</div>

where :

$\Delta_{max} = j\frac{(\varepsilon-1)\pi}{\lambda}I(c_2 - c_1)$ = maximum of ice anisotropy when all the needles are aligned and γ = 90 [degrees] (the needle is transversal to the propagation direction).

I = total ice content, mm

$B = \sin(\beta)\langle\sin[2(90-\gamma)]\rangle$

$C = \langle\cos[2(90-\gamma)]\rangle - 0.5\cos^2(\beta)\langle\cos[2(90-\gamma)]-1\rangle$

$\langle\rangle$ = ensemble average of the parameter.

$c_1 = \frac{1}{1-(\varepsilon-1)a_1}$; $c_2 = \frac{1}{1-(\varepsilon-1)a_2}$; $a_1 = \frac{m}{2(m^2-1)}\left[m - \frac{1}{2\sqrt{m^2-1}}\ln\left(\frac{m+\sqrt{m^2-1}}{m-\sqrt{m^2-1}}\right)\right]$; $a_2 = 1-2a_1$

$\varepsilon = \varepsilon_r - j\varepsilon_i = n^2$ = complex permittivity

$m = a/b > 1$

a,b = major and minor semiaxis of the particle

The values of parameters B and C are given in the following table for some particular cases.

Crystals Orientation	$\langle\gamma\rangle$ deg	B	C
Random Orientation	0	0	$0.5\cos^2(\beta)$
All Aligned	γ_0	$sin(\beta)sin(2\gamma_0)$	$sen^2(\gamma_0)-\cos^2(\gamma_0)sen^2(\beta)$
All Aligned	0	0	$-sen^2(\beta)$
All Aligned	90	0	1

Table 2.4-1: Values of B and C parameters for calculation of ice anisotropy.

The crosspolar discrimination of circular polarisation, for various frequencies, is plotted in Figure 2.4-5 as a function of the total ice content of the cloud [*Paraboni et al., 1997*]. The concurrent attenuation is almost equal to zero.

This shows that the ice crosspolar discrimination can drop below 30 dB, at 18.7, 39.6 and 49.5 GHz for a total ice content of 0.25, 0.15 and 0.1 mm, for a cloud thickness of 500 m. It is to be noted that ice depolarisation increases with frequency.
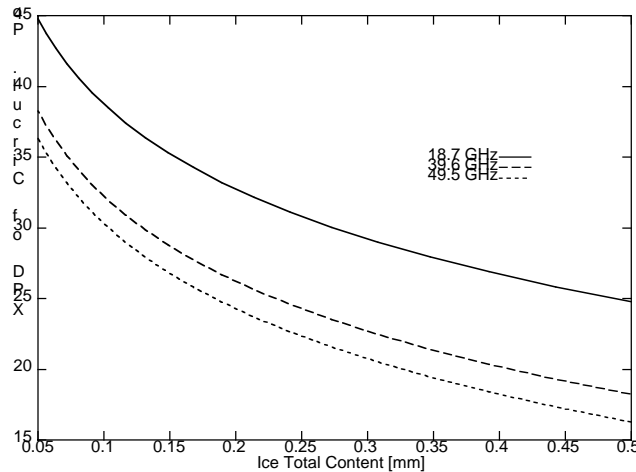

Figure2.4-5: Crosspolar discrimination (XPD) for circular polarisation at Ka and V-Band, versus total ice content. The ice needles are aligned. Rotation angle, γ = 90 º. Link elevation =41º

The value of total ice content in the absence of rain can be estimated using radiosonde measurements of the vertical profile of meteorological parameters. Statistics of the total ice content, derived from radiosonde measurements performed at various locations around the world, are given in the database described in Chapter 2.1. For example, according to this database, the value of total ice content exceeded in Europe for 1 % of the time, ranges from 0.5 to 1.2 mm.

The ice crystals can exhibit higher and faster rotational variations than raindrops, due to aerodynamic and electrostatic effects and this influences the dynamic behaviour of ice depolarisation.

The effect of the rotation of ice crystals on circular and linear polarisations is described in Figure 2.4-6. The considerable reduction of crosspolar discrimination resulting from small fluctuations in the ice crystal orientation can be evaluated, in particular for linear polarisation.

Therefore it is to be expected that ice depolarisation can be characterised by faster fluctuations than during rain depolarisation.
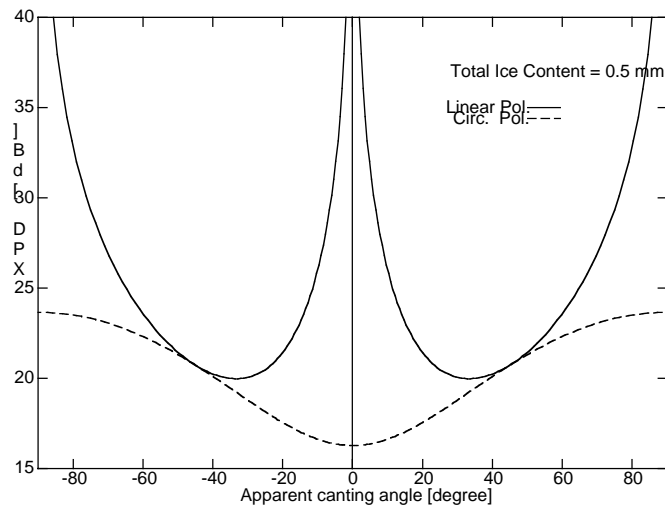
Figure 2.4-6: Cross-Polar Discrimination of linear and circular polarisations due to ice, as a function of the apparent canting angle of the ice cloud, at 50 GHz. The total ice content is 0.5 mm. The link elevation is 41°

An indirect assessment of this model is given by the similarity between the radiosonde estimation and that predicted on the basis of the Olympus and Italsat depolarisation data. As an example, the values of the total ice content in the absence of rain, estimated using the measurements of ice anisotropy and the independent radiosonde measurements, are compared in Figure 2.4-7, [*Martellucci et al., 2000*].

The overestimation of the radiosonde calculation with respect to Italsat measurements can be ascribed to the technique used to estimate cloud ice content. The radiosonde based estimation of ice does not distinguish between spherical and deformed ice crystals. On the contrary the measurements of anisotropy along the path (like the ones performed using the Italsat beacon), are affected only by the fraction of ice crystals which are deformed.

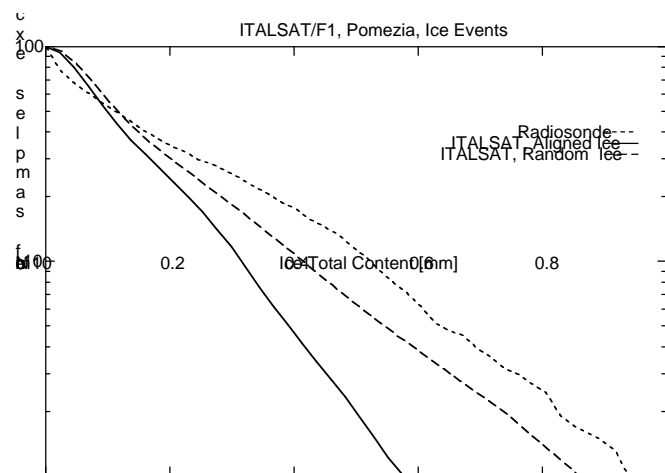*Figure 2.4-7: Cumulative distribution of the ice total content derived from Italsat measurement (using two models for particle alignment) and from local radiosonde data.*

Ice depolarisation during rainfall

Using the model for the medium composed of two kinds of particles (see Section 2.4.2.3), it is possible to calculate the overall depolarisation of the atmosphere, when both rain and ice are

As discussed in the previous chapter, rain and ice anisotropy are related to the rain attenuation and to the ice content respectively. A statistical analysis of anisotropy measurements performed with Olympus and Italsat has shown that ice anisotropy appears to be related to rain intensity, with a different relationship according to the rainfall type (stratiform or convective). This observation suggests the existence of a statistical relationship, between the rain rate at the ground and the content of ice crystals at the top of the raincell, that could be used to derive ice depolarisation during rainfall, from statistics of the rain attenuation.

To this end, the measurements of the atmospheric transfer matrix performed, from April to July 1993 with an Olympus station located in Torino, Italy, have been used by [*Paraboni et al., 1998*] to determine the joint statistics of the rain rate and the total ice content.

The relationship between rain rate and ice content was characterised by two different types of behaviour, according to the rainfall type. During stratiform rainfall the ice total content is related to the rain rate, but its values are similar to those observed in ice clouds. On the other hand the ice total content turned out to be higher during convective rainfall and it exhibited large fluctuations.

The ice total content, along the zenith is given by:

$$I_i = a_i * R + b_i$$
<div align="right">2.4-26</div>

where:

i=20,50 or 80, indicates the values exceeded by 20%, 50% and 80% of the samples (deciles)

For rain rates, R < 30 mm/hr:

a_i = 0.0067, 0.0032, 0.0016;

b_i = 0.07, 0.04, 0.02

For rain rates, R > 40 mm/hr:

a_i = 0;

b_i = 0.7, 0.4, 0.2

This model has been assumed to be valid over the European region and has been used to calculate the values of the total ice content in the Netherlands, using as input the cumulative distribution function of rain rate measured at Eindhoven [*Poiares Baptista & Davies, 1994*]. The data have been compared with estimation of the ice total content based on radiosonde measurements performed in De Bilt, The Netherlands. A fair agreement has been observed between the predicted statistics of the total ice content and the statistics of local radiosonde data (see Figure 2.4-8).
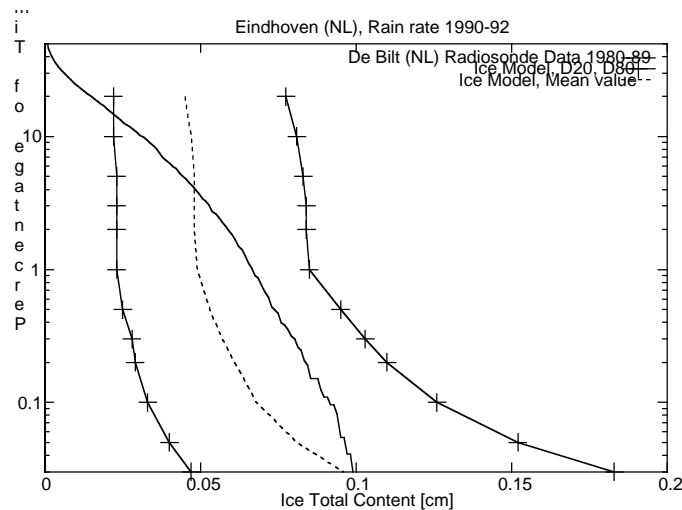
Figure 2.4-8 : Cumulative distribution function of total ice content along the zenith, derived from radiosonde data and predictions derived from the cumulative distribution function of the rain rate.

The crosspolar discrimination due to ice has been estimated by means of equation 2.4-25, assuming that ice crystals are randomly oriented, and compared with Olympus measurements of the crosspolar discrimination performed in Eindhoven at 29.77 GHz [*Dintelmann, 1994; Van de Kamp, 1994*]. The analysis of results in Figure 2.4-9 shows that ice depolarisation in this frequency band can contribute considerably to the overall atmospheric depolarisation, also in the presence of significant rain attenuation.
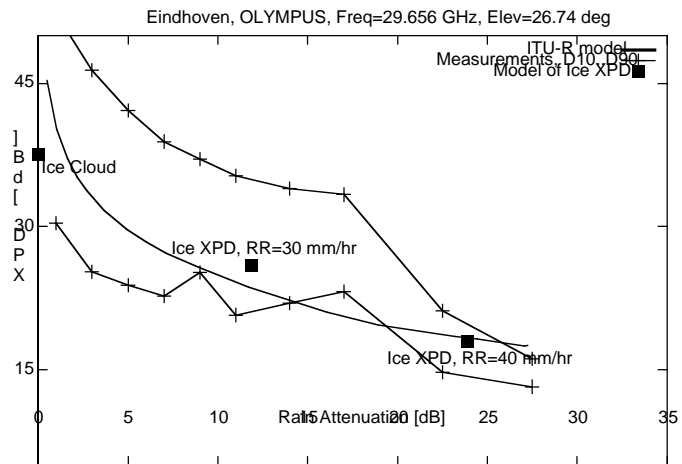
Figure 2.4-9: Joint values of the crosspolar discrimination measured at Eindhoven, the Netherlands, using the Olympus propagation beacon at 29.77 GHz. The results of the ITU-R model are also plotted.

In order to estimate the combination of ice and rain depolarisation effects, statistics are needed of the difference between canting angles of the two families (as discussed in Section 2.4.2.3). Preliminary results from the Italsat propagation experiment at V-Band indicate that this parameter can be described using the normal model, with a mean value near to zero and a standard deviation of about 50º [*Martellucci et al., 2000*].

2.4.3 Models of the XPD-CPA relationship in the Ku-, Ka- and V-Bands

The models described in the following paragraphs give the average relationship between the cross-

crosspolar discrimination. On the other hand these models tend to underestimate the crosspolar discrimination at 30 GHz and in the 40/50 GHz frequency band at low levels of attenuation.

Furthermore, combined statistics of depolarisation and attenuation are necessary to assess the margins of both parameters required for a certain system outage probability [*Mauri et al., 1987; Vasseur et al., 1996*]. Therefore these models are mainly to be used for estimating the CDF of the crosspolar discrimination, using the CDF of rain attenuation as input.

A description is also given of current models of the XPD-CPA relationship for rain and a new model is proposed, based on the assessment of each model against experimental results.

2.4.3.1   The ITU-R Model for Ka-Band and its extension to V-Band

This model permits the evaluation of the cumulative distribution function of crosspolar discrimination by means of an equiprobability relationship between the attenuation and the XPD. Such a relationship can be also assumed as the average relationship between the two parameters [*ITU-R, 1999*].

The following parameters are needed:

A_p =   the rain attenuation exceeded for the percentage of time p, dB.

τ =   tilt angle of the polarisation with respect to the local horizontal [degrees].
           ($\tau = 45°$ for circular polarisation)

f =   frequency, GHz. The model can be used in the range $8 \leq f \leq 35$ GHz

β =   link elevation in degrees. The model can be used in the range $\beta \leq 60°$.

For the percentage of time p the crosspolar discrimination, due to rain, is lower than the value $XPD_{1,p}$:

$$XPD_{1,p} = U - V \log\left(A_p\right) - C_\tau - C_\beta + C_\sigma \qquad \text{2.4-27}$$

where:

$U = 30\log(f) =$ frequency dependent term.

$$V = \begin{cases} 12.8 \cdot f^{0.19}; & 8 \leq f \leq 20\,\text{GHz} \\ 22.6 & ; & 20 \leq f \leq 35\text{GHz} \end{cases} = \text{Attenuation dependent term [*Fukuchi et al., 1984*]}.$$

$C_\tau = 10 \cdot \log[1 - 0.484 \cdot (1 + \cos(4\tau))] = $ Polarisation dependent term.

$C_\beta = 40 \cdot \log(\beta) = $ link elevation dependent term.

$C_\sigma = 0.0052\sigma_p^2 = $ parameter related to the fluctuation of the raindrops canting angle during the events and from event to event. $\sigma_p = 0°, 5°, 10°$

          when p = 1%, 0.1 %, 0.01 %.

It is assumed that due to the effect of ice particles the crosspolar discrimination is lower than $XPD_{2,p}$, for the percentage of time p:

$$XPD_{2,p} = XPD_{1,p} \cdot 0.5 \cdot [0.3 + 0.1\log(p)] \qquad \text{2.4-28}$$

The ice correction parameter has been empirically determined.

The crosspolar discrimination due to rain and ice is lower than the value XPD_ for the percentage

$$XPD_p = XPD_{1,p} - XPD_{2,p} \qquad\qquad 2.4\text{-}29$$

The current ITU-R model of the relationship between rain crosspolar discrimination and attenuation is based on the model originally proposed by [*Nowland et al., 1977*].

The model has been extended to V-Band by recalculating the Olsen and Nowland coefficients to derive rain specific attenuation and phase shift from rain rate [*Martellucci & Paraboni, 1998*]. Those coefficients have been determined using the point matching technique of [*Oguchi, 1983*] for drop scattering amplitude, an oblate spheroid model of the drop shape, a water temperature of zero degrees, the model of [*Ray, 1972*] for water refractive index and the Marshal-Palmer rain drop size distribution. The linear regression is characterised by an error lower than 4%.

Using these coefficients the updated parameters, to be used in equation 2.4-27, for the CPA-XPD relationship at V-Band are :

$$U = 26\log(f) \; ; \qquad V = 20 \qquad\qquad 2.4\text{-}30$$

The new parameters have been tested using the Italsat measurements carried out at Pomezia, Italy (see Chapter 2.6).

2.4.3.2 Model of Fukuchi [*Fukuchi, 1990*]

The model is based on the comparison between the equiprobable relationship between the crosspolar discrimination and the attenuation with the joint statistical distribution of the parameters. The correction factor δ can be used to derive the statistical distribution of XPD, Pr{*XPD<x*}, from the cumulative distribution function of the copolar Attenuation, Pr{*A>a*}:

$$\Pr\{XPD < x\} = \delta \cdot \Pr\{A > a\} \qquad\qquad 2.4\text{-}31$$

where

$x = \mathrm{f}(a)$; theoretical equiprobability relationship between values of XPD due to rain and values of A.

$\delta = \dfrac{100}{100 - \rho} =$ correction factor

$\rho =$ probability of attenuation lower than *a*, conditioned on XPD < x.

The relationship between the correction factor δ and the copolar attenuation, that describes the effect of ice during the different atmospheric conditions, has been experimentally derived from concurrent measurements of beacon depolarisation, attenuation and radar reflectivity performed in Japan:

$$\delta_p = \begin{cases} \delta_0 & ; \quad A_p < A_1 \\[2mm] \dfrac{(A_p - A_1)}{(A_2 - A_1)}(1 - \delta_0) + \delta_0 & ; \quad A_1 < A_p < A_2 \\[2mm] 1 & ; \quad A_p > A_2 \end{cases} \qquad 2.4\text{-}32$$

where :

A_1, A_2 = values of attenuation that correspond to the effective rain rates of 20 and

80 mm/hr.

$\delta_0 = \dfrac{2}{(1-\rho)}$

rainfall events.

α   =   stratus rain ratio. The ratio between the number of stratus rainfall events and the total number of rain events. $\alpha < 1$
(a value of 0.8 was suggested by Fukuchi).

The percentage of time during which the crosspolar discrimination due to rain and ice is lower than XPD_p, $Perc\{XPD < XPD_p\}$, is calculated by multiplying the percentage of time, p, during which the Crosspolar Discrimination due to rain ice is lower than XPD_p, calculated according to the ITU/R model (see equation 2.4-27, and the extension up to V-Band in equation 2.4-30), for the corresponding ice correction factor δ_p, derived using the cumulative distribution function of attenuation A_p:

$$Perc\{XPD < XPD_p\} = \delta_p \cdot p \qquad \text{2.4-33}$$

The model has been checked against measurements performed in Japan with ETS-II and the BSE propagation experiments, with a good accuracy at 11.5 GHz (linear and circular polarisation) and a fixed underestimation of about 6 dB at 34 GHz. This underestimation has been ascribed to the lack of accuracy of the attenuation statistical distribution. The model has also been checked using the ITU/R database of XPD distribution, that contains data measured at frequencies from 11 to 35 GHz, and the prediction error was ±10% for the majority of experiments contained in the database.

2.4.3.3   *Dissanayake, Haworth, Watson analytical model* [*Dissanayake et al., 1980*]

The model is valid in the range 9-30 GHz and determines the relationship between rain crosspolar discrimination and attenuation by means of small amplitude and phase approximations of the rain transmission matrix.

$$XPD_{1,p} = U' - V'\log(A) - C_\beta - C'_\tau + C'_\sigma \qquad \text{2.4-34}$$

where :

$U' = 84.8 - 88.8xf^y + (50.32xf^y - 21.9)\log(f) = $ frequency dependent term (x = 0.759, y = 0.08).

$V' = 20$ =   attenuation dependent term.

$C_\beta = 40 \cdot \log[\cos(\beta)]$ =   link elevation dependent term.

$C'_\tau = 20\log[\sin(2\tau)]$ =   polarisation dependent term.

$C_\sigma = 17.37\sigma^2$ =   parameter related to the distribution of the raindrop canting angle.

σ   =   r.m.s raindrop canting angle [rad].

The depolarisation due to ice is determined, modelling the ice needles as prolate spheroids that lie in the horizontal plane and applying Rayleigh scattering. The complex depolarisation ratio of linear and circular polarisation can be simplified assuming a small argument approximation and random orientation of the needles.

$$|X_I| \approx \frac{\Delta_I}{2}\cos^2\left(\frac{\beta}{2}\right)\sin(2\tau)$$

$$Arg(X_I) \approx \frac{\pi}{2} - \frac{\Delta_I}{2}\cos^2\left(\frac{\beta}{2}\right)\cos(2\tau) \qquad \text{2.4-35}$$

$$X_c \approx \frac{i\Delta_I}{2}\cos^2\left(\frac{\beta}{2}\right)\exp(j2\tau)$$

where:

$\Delta_I = (k_1 - k_2)l$ $\quad = \quad$ anisotropy of ice crystals, [rad].

$k_i = \frac{3\pi}{\lambda}Vu_i$ $\quad = \quad$ propagation constants of the polarisation parallel (i=1) and perpendicular (i=2) to the symmetry axis of the particle.

l $\quad = \quad$ path length, m

V $\quad = \quad$ total volume of ice/m^3. The total ice content is V*l.

λ $\quad = \quad$ wavelength, m.

u_i $\quad = \quad$ anisotropy coefficients for Rayleigh scattering.

For ice needles $u_1 = 0.7228 - i0.00285$, $u_2 = 0.3468 - i0.00066$.

As discussed earlier, the effect of the melting layer is ignored, because it is assumed to be an isotropic medium, and the combined effect of rain and ice particles on the complex depolarisation ratio is determined by discarding the products of cross-polar terms. The overall depolarisation is obtained by adding the complex depolarisation ratio.

$$X_I \approx X_I(rain) + \frac{T_{22}(rain)}{T_{11}(rain)}X_I(ice)$$
$$X_c \approx X_c(rain) + X_c(ice)$$

2.4-36

where:

$T_{11}(rain)$, $T_{22}(rain)$ = Copolar terms of the rain transmission matrix

2.4.3.4 Other models of the XPD-CPA relationship due to rain

In the literature other models can be found that describe the average relationship between copolar attenuation and the crosspolar discrimination due to rain.

Chu Model [Chu, 1982]

$$XPD_{1,p} = U - 20\log(A_p) - C_\tau - C_\beta + C_\sigma - C_x + 11.5$$

2.4-37

where :

$U = 20\log(f)$ $\quad$ = frequency dependent term.

$C_\tau = 10\cdot\log\{0.5\cdot[1 - \cos(4\tau)\exp(-0.0024\sigma_\varphi^2)]\}$ = Polarisation dependent term.

σ_φ $\quad$ = standard deviation of raindrops during a thunderstorm, ($\sigma_\varphi = 3$ degrees)

$C_\beta = 40\cdot\log[\cos(\beta)]$ $\quad$ = link elevation dependent term.

$C_x = 0.075\cdot\cos^2(\beta)\cdot\cos(2\tau)\cdot A_p$ = difference between horizontal and vertical polarisation.

$C_\sigma = 0.0052\sigma_p^2$ $\quad$ = parameter related to the fluctuation of the raindrop canting angle during the events and from event to event.

Stutzman and Runyon model [*Stuzman and Runyon, 1984*]

$$XPD_{1,p} = U - 19\log(A_p) - C_\tau - C_\beta + C_\sigma + 9.5 - \log(r) \tag{2.4-38}$$

where :

$U = 17.3\log(f)$ = frequency dependent term.

$C_\tau = 10 \cdot \log\{0.5 \cdot [1 - \cos(4\tau)\exp(-0.0024\sigma_\varphi^2)]\}$ = polarisation dependent term.

σ_φ = standard deviation of raindrops during a thunderstorm, ($\sigma_\varphi = 3$ degrees)

$C_\beta = 42 \cdot \log[\cos(\beta)]$ = link elevation dependent term.

$C_\sigma = 0.0052\sigma_p^2$ = parameter related to the fluctuation of the raindrop canting angle during the events and from event to event.

r = fraction of non-spherical raindrops (see equation 2.4-19)

Nowland, Sharofsky and Olsen (NOS) model [*Nowland et al., 1977*]

$$XPD_{1,p} = U - V\log(A_p) - C_\tau - C_\beta + C_\sigma + 4.1 + (V - 20)\log(L) \tag{2.4-39}$$

where :

$U = 26\log(f)$ = frequency dependent term.

$V = \begin{cases} 20; & 8 \le f \le 15\text{GHz} \\ 23; & 15 \le f \le 35\text{GHz} \end{cases}$ = attenuation dependent term (as ITU-R).

$C_\tau = 20 \cdot \log|\sin(2\tau)|$ = polarisation dependent term.

$C_\beta = 40 \cdot \log[\cos(\beta)]$ = link elevation dependent term.

$C_\sigma = 0.0052\sigma_p^2$ = parameter related to the fluctuation of the raindrop canting angle during the events and from event to event.

L = path length through rain (an empirical relationship has been suggested by the authors).

Van de Kamp Model [*Van de Kamp, 1999*]

The parameters of this model have been determined by comparing a general XPD-CPA relationship with a large group of measurements performed at 29 different locations. The frequencies of the measurements vary from 11 to 50 GHz, and the elevation angles from 3º to 50º. The polarisation angles vary from 0º to 180º, including also measurements at circular polarisation. The dependency of each parameter has been assessed separately by selecting each time a group of measurements which are equal in all but one parameter.

The general equation that has been tested, using the measurements, is:

$$XPD_{1,p} = C\log(f) - V\log(A_p) - C_\tau - D\log(\beta) + C_\sigma - C_x + S \tag{2.4-40}$$

where:

the model parameters are C, V, D and S

$C \cdot \log(f) = U$ = frequency dependent term.

τ = polarisation tilt angle [degree]

C_τ = polarisation dependent term.

β = link elevation [degree]

$D \log[\cos(\beta)] = C_\beta$ = link elevation dependent term.

$C_x = 0.075 \cdot \cos^2(\beta) \cdot \cos(2\tau) \cdot A_p$ = difference between horizontal and vertical polarisation

[*Chu, 1982*].

$C_\sigma = 0.0052 \sigma_p^2$ = parameter related to the fluctuation of the raindrop canting angle.

S = constant value.

From the separate assessment of each equation with experimental values, we have:

C	V	D	S
20 (11.6 to 29.7 GHz)	16.3	41	8

Table2.4-2: Parameters of the Van de Kamp model of rain XPD-CPA

For the experiments at frequencies from 28.5 to 49.5 GHz it was found that the correlation is maximised for C equal to 25, in good agreement with the theoretical assessment performed in Section 2.4.3.1 (C=26).

In Figure 2.4-10, the model of equation 2.4-40 and all measurements used to perform model assessment are plotted, normalised according to the following equation:

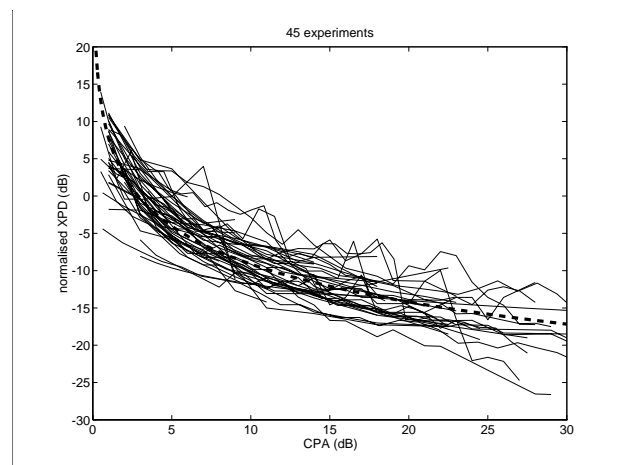$$XPD_{norm} = XPD - \left(U - C_\tau - C_\beta - C_x \right) \qquad \text{2.4-41}$$

Figure 2.4-10: General test of the model: normalised XPD versus CPA, for 45 experiments; and a curve fitted to the results (thick dashed line).

2.4.4   The effect of depolarisation on radio communication systems

In order to estimate the effect of atmospheric depolarisation on radio communication systems, a distinction must be made between full co-channel frequency reuse and frequency-interleaved reuse

[*Alnutt, 1989*]. In Figure 2.4-11 a number of carriers are shown within the satellite transponder bandwidth, showing the frequency-polarisation allocation scheme.
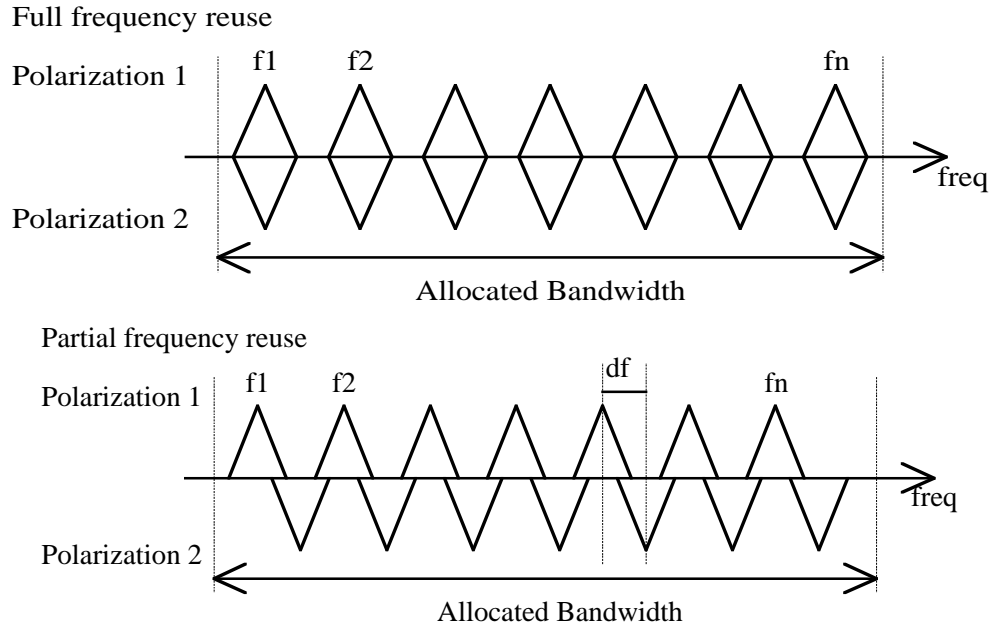

Figure 2.4-11: Spectrum utilisation for full or frequency interleaved frequency reuse. The frequency offset df describes the overlapping of the communication bands

The atmospheric depolarisation gives rise to interference between adjacent channels. This interference can be described, to a first approximation, as white noise not correlated with the signal. Therefore atmospheric depolarisation reduces the signal to noise power ratio.

The total signal to noise ratio, (C/N)$_T$, in a satellite communication links is given by:

$$\frac{1}{(C/N)_T} = \frac{1}{(C/N)_U} \frac{1}{(C/N)_U} \frac{1}{(C/N)_{IM}} \frac{1}{(C/I)}$$

2.4-42

where :

$(C/N)_U$ = signal to noise ratio on the uplink from ground to the satellite.

$(C/N)_D$ = signal to noise ratio on the downlink from the satellite to ground.

$(C/N)_{IM}$ = signal to noise ratio due to intermodulation products between adjacent channels.

(C/N) = signal to noise ratio due to interference between adjacent channels, e.g. atmosphere, antennas.

The terms are numerical power ratios.

The reduction of the signal to noise ratio (C/N), with respect to the nominal level $(C/N)_{nom}$, due to the joint effect of the atmospheric depolarisation, XPD, and attenuation, A, can be determined using the following relationship:

$$C/N = -10\log\left[10^{-\left(\frac{(C/N)_{nom}-A}{10}\right)} + 10^{-\frac{XPD}{10}}\right]$$

2.4-43

These relationships and the type of modulation employed by the radiocommunication system, define a bi-dimensional set of attenuation, A, and cross-polar discrimination values, XPD, that give rise to a bit error rate (BER) that is still below the desired threshold, e.g. 10^{-6}. This set of values, D, is formed by the joint values of A and XPD that satisfy the following relationship:

$$f(A, XPD) > T(BER)$$ <div style="float:right">2.4-44</div>

where :

$f(A, XPD)$ = function of A, attenuation, and XPD, crosspolar discrimination.

$T(BER)$ = threshold value which depends on the required Bit Error Rate (BER) and on the system characteristics

The behaviour of attenuation and cross polar discrimination can be described by their joint probability function $p(A, XPD)$, where $p(A, XPD)dAdXPD$ is the probability that attenuation and crosspolar discrimination are contained in the following ranges: $A \leq a < A + dA$; $XPD \leq d < XPD + dXPD$.

Therefore the probability that the communication system is characterised by a BER lower than the required threshold, in the presence of atmospheric attenuation and crosspolar discrimination, is given by the following relationship:

$$\Pr(BER) = \iint_D p(A, XPD)dAdXPD$$ <div style="float:right">2.4-45</div>

In order to estimate the performance of a frequency reuse communication system, the joint probability density function $p(A, XPD)$ for the link site, frequency, adopted polarisation and geometry is needed [*Mauri et al., 1987*].

2.4.5   References

[*Alnutt, 1989*]
Alnutt J., "Satellite-to-ground Radiowave Propagation", IEE Electromagnetic Waves Series, 29, 1989

[*Amaya, 1995*]
Amaya-Byrne C., "Depolarisation due to troposphere and its impact on satellite-to-earth communications", PhD Thesis, Université Catholique de Louvain-la-Neuve, Belgium, June 1995.

[*Aresu et al. 1995*]
Aresu A., A. Martellucci, A. Paraboni, R. Polonio, "Theoretical and experimental channel characterisation of spatial links at 20 and 50 GHz", Proceedings of 7th International Union of Radio Science Commission F Open Symposium "Wave Propagation and remote sensing", Ahmedabad, India, 20-24 November 1995, pp. 303-306.

[*Aresu et al. 1994*]
Aresu A., E. Damosso, A. Martellucci, L. Ordano, A. Paraboni, "Depolarisation of electromagnetic waves due to rain and ice: theory and experimental results", Alta Frequenza, Vol. 6, N. 6, November-December 1994, pp 70-75

[*Aresu et al. 1993*]
Aresu A., Martellucci A. and Paraboni A., "Experimental assessment of rain anisotropy and canting angle in horizontal path at 30 GHz", IEEE Trans. on Antennas and Propagation, Vol. 41, No. 9, pp. 1331-1335, September 1993

[*Capsoni & Paraboni, 1972*]
Capsoni C.and Paraboni A., "Depolarisation of an EM Wave traveling through a stratified aerosol of non spherical scatterers", AGARD EPP Tech. Meeting, Gausdal Norway, Sept. 1972.

[*Capsoni et al., 1981*
Capsoni C., Paraboni A., Fedi F., Maggiori D.,"A model oriented approach to measure rain induced crosspolarisation", Annal. de Telecommunicat., Vol. 36, n. 1-2, Jan-Feb. 1981.

[*Chu, 1982*]
Chu, T. S., "A semi-empirical formula for microwave depolarisation versus rain attenuation on earth-space paths", IEEE Trans. Commun., COM-30(12), 2550-2554, 1982.

[*Dintelmann, 1994*]
Dintelmann F. (Editor), "Reference Book on Depolarisation", OPEX- ESA WPP-083, 1994.

[*Dissanayake et al., 1980*]
Dissanayake A. W., Haworth D. P. and Watson P. A, "Analytical models for cross-polarisation on earth space radio paths for frequency range 9-30 GHz" H., Ann. Telecommunic., 35, n° 11-12, 1980, pp 398-404.

[*Fukuchi, 1990*]
Fukuchi H., "Prediction of depolarisation distribution on earth-space paths", IEE Proceedings, Vol. 137, Pt. II, n. 6, December 1990.

[*Fukuchi et al., 1984*]
Fukuchi, H., J. Awaka and T. Oguchi, "Improved theoretical formula for the relationship between

[*ITU-R, 1999*]
ITU-R, P 618-6, "Propagation data and prediction methods required for the design of Earth-space telecommunication systems", 1999,

[*Martellucci et al., 1993*]
Martellucci A., Mauri M. and Paraboni A., "The physical basis of depolarisation", Proceedings of Olympus Utilisation Conference, (Sevilla, Spain), 20-22 April 1993, pp. 573-581.

[*Martellucci & Paraboni, 1994*]
Martellucci A. and Paraboni A., "Modelling of Depolarisation due to Hydrometeors: Utilisation of multipolarisation radiowave beacon for estimation of quasi-phyisical parameters", Proc. of PIERS 94, ESA, Noordwijk,The Netherlands, July 11-15 1994.

[*Martellucci & Paraboni, 1998*]
Martellucci A. and A. Paraboni, "Test and Development of Models of Atmospheric Crosspolar Discrimination for Satellite Communication Systems at Ka- and V-Band", Proceed. of the first international Workshop on Radiowave Propag. Model. for SatCom Serv. at Ku-band and above, Estec, Noordwijk, The Netherlands, 28-29 October 1998

[*Martellucci et al., 2000*]
Martellucci A., Paraboni A. and Filipponi M. "Measurements and modeling of rain and ice depolarisation on spatial links in the Ka- and V-Bands", invited paper, AP2000 Millennium Conference on Antennas and Propagation, Davos, Switzerland, 9-14 April 2000.

[*Mauri et al., 1987*]
Mauri M., A. Paraboni and D. Tarducci, "Depolarisation Measurements and their use in the determination of dual polarisation links performance", Alta Frequenza, Vol. LVI, No. 1-2, Jan.-Apr. 1987

[*Nowland et al., 1977*]
Nowland W.L., Olsen R. L., Shkarofsky, "Theoretical relationship between rain depolarisation and attenuation", Electronics Letters, Vol. 13, No. 22, pp 676-678, 27 October 1977

[*Oguchi, 1983*]
Oguchi T., "Electromagnetic wave propagation and scattering in rain and other hydrometeors", Proc. IEEE, Vol. 71, No. 9, pp. 1029-1078, September 1983.

[*Paraboni et al. 1997*]
Paraboni A., A. Martellucci and R. Polonio, "A probabilistic model of rain and ice depolarisation based on the experimental estimation of the atmospheric ice content", Proc SBMO/IEEE International Microwave and Optoelectronics Conference, Natal, Brazil, 11-14 August 1997, pp 707-712

[*Paraboni et al., 1998*]
Paraboni A., A. Martellucci, R. Polonio, "Statistical Modelling of Depolarisation due to Rain and Ice During Thunderstorms Based on the Italsat and Olympus Measurements", Proc. 8th URSI Commission F Triennial Open Symposium, , Aveiro, Portugal, 22-25 September 1998, pp. 288-291.

[*Poiares Baptista & Davies, 1994*]
Poiares Baptista, J.P.V. and Davies P. G. (Editors), "OPEX: Reference Book on Attenuation measurements and prediction", ESA WPP-83, November 1994.

[*Poiares Baptista, 1994*]
Poiares Baptista J.P.V. (Editor), "Reference Book on Radar", OPEX- ESA WPP-083, November 1994.

[*Ray, 1972*]
Ray P. S., "Broad Band Complex refractive index of ice and water", Applied Optics, Vol. 11, No. 8, 1972.

[*Stuzman and Runyon, 1984*]
Stutzman, W. L., and D. L. Runyon, "The relationship of rain- induced cross-polarisation discrimination to attenuation for 10 to 30 GHz earth-space radio links", IEEE Trans. Antennas Propagat., AP-32(7), 705-710, 1984.

[*Van de Kamp, 1999*]
Van de Kamp M. (1999), "Depolarisation due to rain: the XPD-CPA relation", Int. J. Sat. Com., Vol. 9, Issue 3, pp. 285-301, 2001.

[*Vasseur et al., 1996*]
Vasseur, H., I. Adams, C. Amaya, and D. Vanhoenacker (1994), "Comparison of Yearly Statistics with CCIR Prediction Methods", Proceedings of 21st Meeting of Olympus Propagation Experimenters, OPEX XXI, Louvain-la-Neuve, Belgium, May 1994, 80-89.

2.4.6 Appendix to Chapter 2.4: Description of Polarisation

A plane wave is assumed, propagating along the z direction. The complex amplitude of the electric field is $\mathbf{E} = E_x\mathbf{x} + E_y\mathbf{y}$, where xyz is a left hand reference system. An $\exp(+j\omega t)$ time convention is assumed and is suppressed.

2.4.6.1 *Complete description of the electric field*

The electric field is given by:

$$E_x = a_x e^{j\delta_x}$$
$$E_y = a_y e^{j\delta_y}$$

A-1

The state of polarisation is described by the parameters a_x, a_y and δ, where: $\delta = \delta_y - \delta_x$, $-\pi < \delta \leq \pi$.

Polarisation	a_x	a_y	δ
Linear	(0, +00)	(0, +00)	$m\pi$
Linear X	0	(0, +00)	$m\pi$
Linear Y	(0, +00)	0	$m\pi$
Linear ±45°	$a_x = \pm a_y$	$a_x = \pm a_y$	$m\pi$
Right Handed Circular	$a_x = a_y$	$a_x = a_y$	$-\dfrac{\pi}{2} + 2m\pi$
Left Handed Circular	$a_x = a_y$	$a_x = a_y$	$+\dfrac{\pi}{2} + 2m\pi$

Table A-1: State of polarisation according to the complete description of the electric field

where m is an integer.

2.4.6.2 *Reduced Parameters of the Electric Field*

The electric field can be described as:

$$\mathbf{E} = E_0\left[\cos(\alpha)\mathbf{x} + sen(\alpha)e^{j\delta}\mathbf{y}\right]$$

A-2

The state of polarisation is described by the parameters α and δ, where $0 \leq \alpha \leq \pi/2 : -\pi < \delta \leq \pi$

Polarisation	α	δ
Linear X	0	π
Linear Y	$\pi/2$	0
Linear ±45°	$\pi/4$	0, π
Right Handed Circular	$\pi/4$	$-\pi/2$
Left Handed Circular	$\pi/4$	$+\pi/2$

Table A-2: State of polarisation described using the reduced parameters of the electric field.

2.4.6.3 *Ellipse of polarisation*

The ellipse of polarisation of the electric field can be described using the length of the semiaxes, a and b, the sense of rotation of the electric field along the ellipse and the canting of the polarisation ellipse with respect to x axis.

a = length of the major semiaxis of the ellipse

b = length of the minor semiaxis of the ellipse

$r = (b/a)$ = axial ratio of the ellipse. $0 \le r < +\infty$

$\chi = \pm \arctan(r)$ = ellipticity, (+ = left handed polarisation, - = right handed polarisation).
$-\pi/4 \le \chi \le +\pi/4$

ψ = Canting of the ellipse with respect x axis; $-\pi/2 < \psi \le +\pi/2$.

These parameters can be calculated using the following relationships :

$$a = \frac{1}{2}\left[a_x^2 + a_y^2 + \sqrt{a_x^4 + a_y^4 + 2a_x^2 a_y^2 \cos(2\delta)} \right] \qquad \text{A-3}$$

$$b = \frac{1}{2}\left[a_x^2 + a_y^2 - \sqrt{a_x^4 + a_y^4 + 2a_x^2 a_y^2 \cos(2\delta)} \right] \qquad \text{A-4}$$

$$\tan(2\psi) = \tan(2\alpha)\cos(\delta) \qquad \text{A-5}$$

Polarisation	χ	ψ
Linear	0	$(0, \pi/2]$
Linear X	0	0
Linear Y	0	$\pi/2$
Linear ±45°	0	$\pm\pi/4$
Right Handed Circular	$-\pi/4$	not defined
Left Handed Circular	$+\pi/4$	not defined

Table A-3:. State of polarisation described using the ellipse of polarisation.

2.4.6.4 *Stokes' Parameters*

The Stokes' parameters , S_0, S_1, S_2, and S_3, are defined by the following relationships:

$$S_0 \equiv a_x^2 + a_y^2 = a^2 = S_1^2 + S_2^2 + S_3^2$$

$$S_1 \equiv a_x^2 - a_y^2 = a^2 \cos(2\alpha) = a^2 \cos(2\chi)\cos(2\psi)$$

$$S_2 \equiv 2a_x a_y \cos(\delta) = a^2 \cos(2\alpha)\cos(\delta) = a^2 \cos(2\chi)sen(2\psi) \qquad \text{A-6}$$

$$S_3 \equiv 2a_x a_y sen(\delta) = a^2 sen(2\alpha)sen(\delta) = a^2 sen(2\chi)$$

The vector $\mathbf{S} = (S_1, S_2, S_3)$ can be used to describe the polarisation. The extremes of this vector are located on a sphere, that is called the Poincaré sphere, whose radius is equal to S_0. Orthogonal polarisations are described by opposite Stokes' vectors, making the identification simple.

Polarisation	S
Linear	$(S_1, S_2, 0)$
Linear X	$(S_0, 0, 0)$
Linear Y	$(-S_0, 0, 0)$
Linear ±45°	$(0, \pm S_0, 0)$
Right Handed Circular	$(0, 0, -S_0)$
Left Handed Circular	$(0, 0, S_0)$

Table A-4: State of polarisation described using the Stokes' parameters.

2.4.6.5 *Complex Polarisation Factor*

The complex polarisation ratio, p, is the ratio between the component of the electrical field:

$$p = \frac{E_y}{E_x} = \tan(\alpha)e^{j\delta} \qquad \text{A-7}$$

This complex parameter represents the stereographic projection of a point on the Poincaré sphere on the plane orthogonal to axis S_1, with $\text{Re}(p)$ parallel to S_2 and $\text{Im}(p)$ parallel to S_3.

Polarisation	Re(p)	Im(p)
Linear	$[0,+\infty)$	0
Linear X	0	0
Linear Y	∞	0
Linear ±45°	±1	0
Right Handed Circular	0	-1
Left Handed Circular	0	+1

Table A-5: State of polarisation described using the complex polarisation factor.

2.4.6.6 *Complex canting angle of the polarisation ellipse*

The complex canting angle of the polarisation is given by the following relationship:

$$\tan(\Phi) = p \qquad \text{A-8}$$

This parameter is related to the parameters of the polarisation ellipse by the following relationships:

$\text{Re}(\Phi) = \psi$ = canting angle of the ellipse with respect x axis. $-\pi/2 < \text{Re}(\Phi) \le +\pi/2$

$r \equiv a/b = \tanh[\text{Im}(\Phi)]$ = axial ratio of the ellipse. $0 \le r < +\infty$

Polarisation	Re(Φ)	Im(Φ)
Linear	(0, π/2]	0
Linear X	0	0
Linear Y	π/2	0
Linear ±45°	± π/4	0
Right Handed Circular	0	-∞
Left Handed Circular	0	+∞

Table A-6: State of polarisation described using the complex canting angle.